The effect of metal oxide nanoparticles on cardiovascular system

Yuka Suzuki
Doctoral Course
Graduate School of Regional Innovation Studies,
Mie University

Contents

page

1. Introduction

1-1 Nano safety

According to the European Commission, nanomaterial is defined as a material containing particles with one or more external dimensions in the size range of 1 - 100 nm (European Commission., 2012, The Royal Society & The Royal Academy of Engineering., Fig.1).

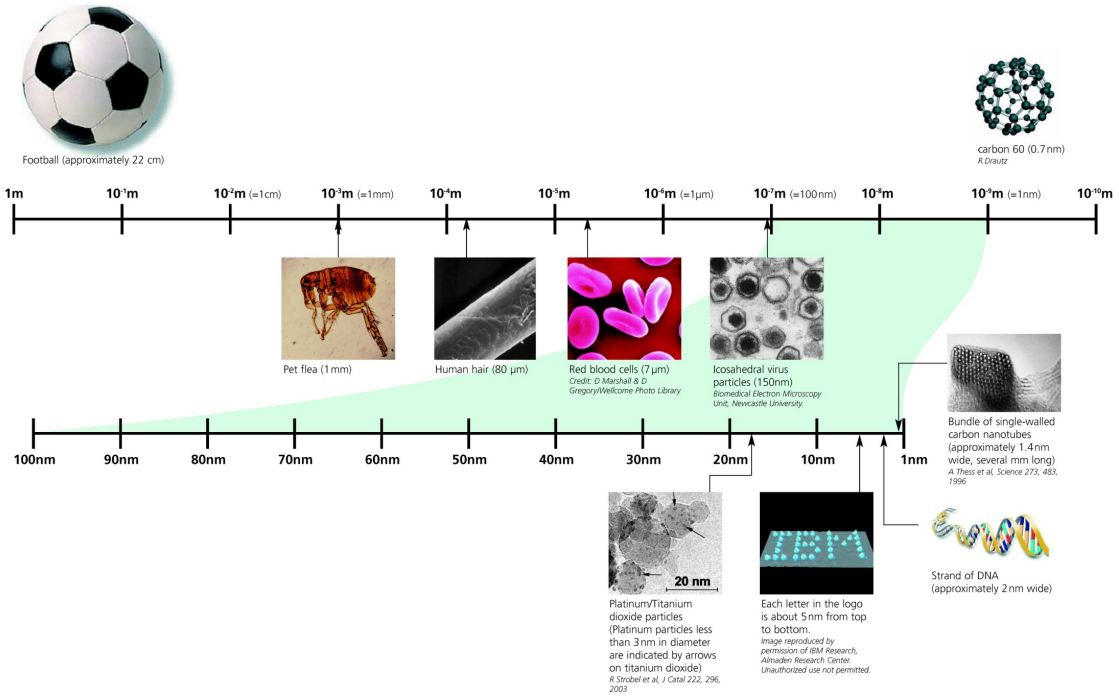

Fig.1. The scale of nanomaterial. (The Royal Society & The Royal Academy of Engineering.,2004)

The remarkable revolution in nanotechnology shows promising potential applications of manufactured nanomaterials in a variety of areas including engineering, medicine,

consumer, and information technology (Donaldson et al., 2004 and Warheit et al., 2007). On the other hand, safety evaluation of manufactured nanomaterials is urgently required because of the considerable probability of occupational and environmental exposure throughout the product chain during manufacture, application and waste management (Donaldson et al., 2004 and Sager et al., 2009). Furthermore, there is increasing concern that the novel physico-chemical properties of nanomaterials that are different from those of bulk materials might have unpredictable health effects (Ema et al., 2010 and Nel et al., 2006).

Both *in vivo* and *in vitro* studies demonstrated that the higher toxicity of nanomaterials was correlated with the relatively larger surface area derived from their smaller sizes (Sager et al., 2007, Sager et al., 2008, Shvedova et al., 2005, Wick et al., 2007 and Yamamoto et al., 2006). However, nanomaterials tend to agglomerate into micrometer-sized structures in aqueous media, subsequently exerting different biological effects compared to well-dispersed ones, probably due to the ineffective surface area delivered by the poor dispersed suspension (Bihari et al., 2008, Maynard et al., 2005, Oberdörster et al., 2005 and Tsuji et al., 2006). Therefore, the selection of suitable dispersion methods is important for accurate evaluation of toxicological responses to nanomaterials.

In safety research on nanomaterials, sonication is the most widely used procedure to accomplish a suspension (Kobayashi et al., 2009, Li et al., 2007, Liang et al., 2009 and Muller et al., 2009). Cavitation from alternating high and low pressure cycles provides energy that facilitates the disruption of agglomerates. Agglomerates of particles bound together by relatively weak forces, such as Van der Waals forces, can be fragmented

by sonication, while aggregates created by stronger chemical bonds are difficult to be broken down (Taurozzi et al., 2011). Instead of electrostatic stabilization, steric stabilization by adding stabilizers into the suspension is often used to maintain homogeneous dispersion induced by sonication (Fig.2).

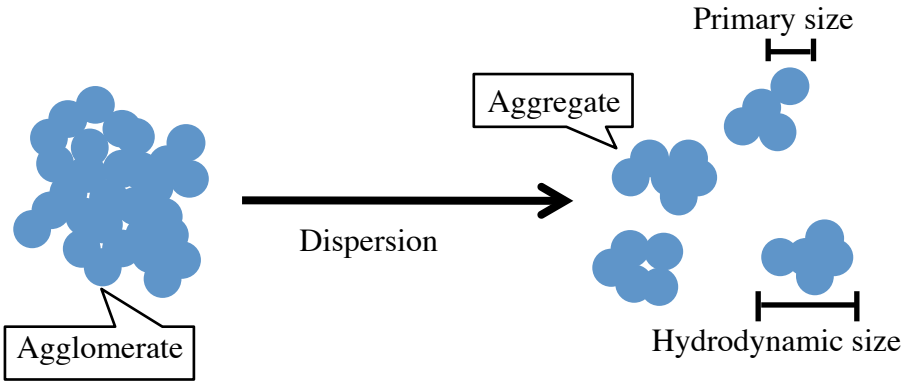

Fig.2. Schema of primary particles, agglomerates, and aggregates.

Pulmonary surfactant, albumin, cell culture medium, and serum have been reported to prevent nanomaterials from approaching each other by protein corona, contributing to the suppression of gross cluster formation and the improvement of suspension stability (Bihari et al., 2008, Murdock et al., 2008 and Schulze et al., 2008).

1-2 Translocation to bloodstream

Exposure to nanomaterials can occur through different routes: inhalation (respiratory tract), ingestion (gastrointestinal tract), direct contact with the skin, and injection (blood circulation) (Oberdörster et al., 2005). Previous studies suggested that inhaled particles in the lungs may cause systemic inflammation through oxidative stress, which mediates endothelial dysfunction and atherosclerosis (Mills et al., 2007).

Moreover, since nanomaterials are 100 nm or less in size, they may reach the deeper respiration area of lung (Fig.3. Modified image from website of Ministry of the Environment).

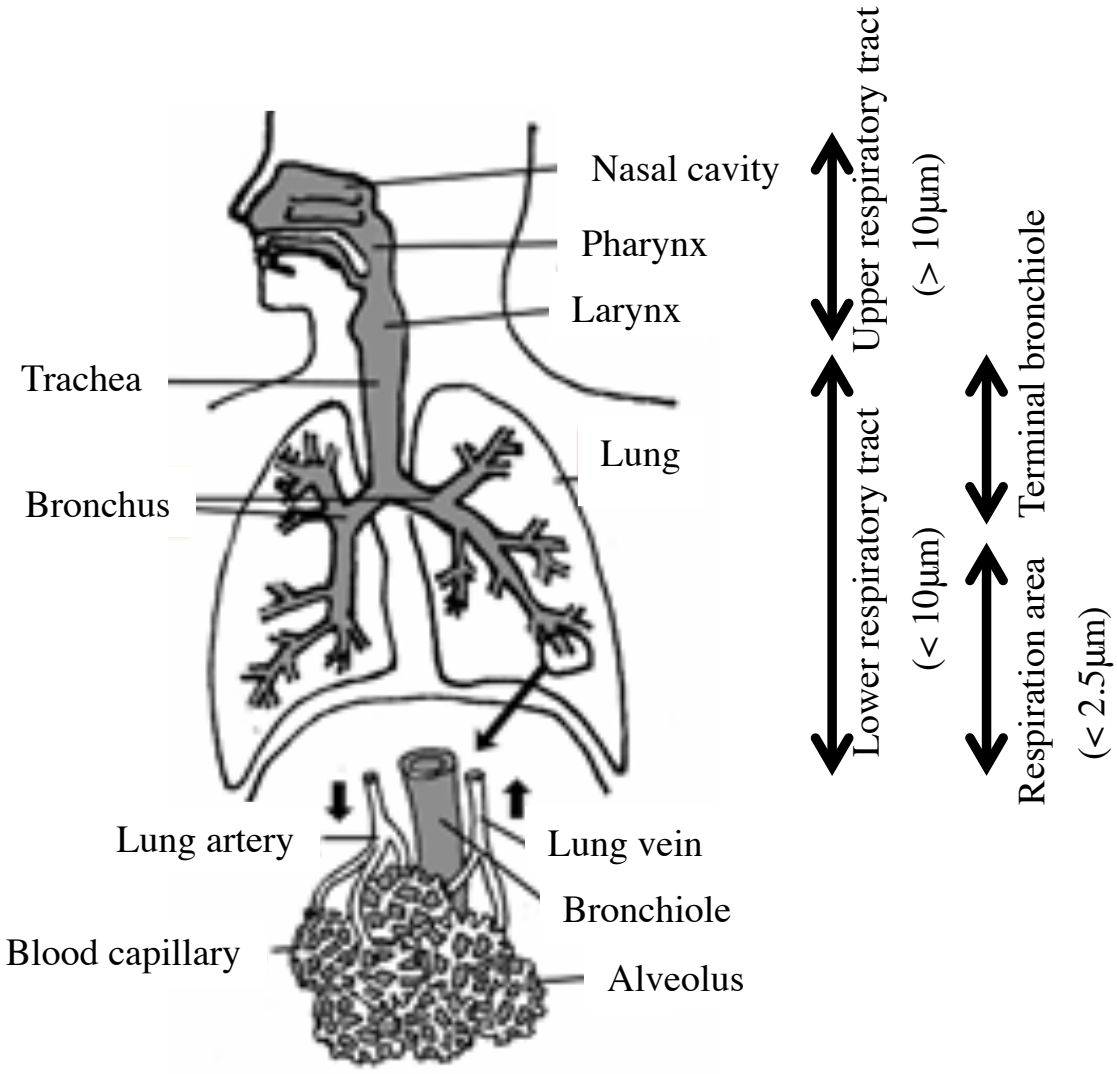

Fig.3. Range of particle deposition and human respiratory system. (Modified image from website of Ministry of the Environment).

In addition, these particles are also thought to increase blood coagulability through the activation of platelets and enhancement of autonomic nervous system via pulmonary reflexes, leading to increased risk of cardiovascular diseases (Seaton et al., 1995). Recent studies demonstrated that nano-sized particles can cross the pulmonary epithelial barrier and enter the bloodstream (Choi et al., 2010, Kreyling et al., 2002 and Nemmar et al., 2002). These results suggest that nanoparticles could be taken up by endothelial cells and potentially interact directly with endothelial cells to induce injury and inflammation. The results of animal studies on alveolar translocation of nanoparticles suggest the existence of the same pathway in humans; however, the extent of extrapulmonary translocation is highly dependent on particle surface characteristics/chemistry, in addition to particle size. Translocation to the peripheral circulation could provide a mechanism for the direct effect of such particles on the cardiovascular system.

1-3 Effects of nanomaterials on human health

Evidence based on epidemiological and toxicological studies indicates that high concentrations of particle masses <2.5 μm (PM2.5) are associated with high risk of pulmonary complications, cardiovascular events, and death from cardiovascular disease (Araujo et al., 2008, Mar et al., 2000, Miller et al., 2007, Mills et al., 2007 and Peters et al., 2001). The recent explosion in the field of nanotechnology provides promising potential applications of manufactured nanomaterials in a variety of areas (Donaldson et al., 2004). It has been demonstrated that the relative surface area of ultrafine carbon black or titanium dioxide (TiO_2) particles correlates with the

degree of their toxicity (Hohr et al., 2002, Sager et al., 2008 and Yamamoto et al., 2006). Some kinds of nanomaterials are also considered to generate reactive oxidant species, resulting in the induction of oxidative stress and inflammation (Nel et al., 2009 and Xia et al., 2006). Oxidative stress is known to be involved in the pathogenesis of cardiovascular diseases, such as hypertension and atherosclerosis (Noma et al., 2007 and Taniyama and Griendling, 2003). Therefore, there is a concern that nanomaterials could have a major impact on the cardiovascular system. However, the effects of exposure to newly developed metal oxide nanoparticles on the cardiovascular system remain elusive.

1-4 References

J.A. Araujo, B. Barajas, M. Kleinman, X. Wang, B.J. Bennett, K.W. Gong, M. Navab, J. Harkema, C. Sioutas, A.J. Lusis, A.E. Nel. Ambient particulate pollutants in the ultrafine range promote early atherosclerosis and systemic oxidative stress. Circ. Res., (2008) 102, pp. 589–596.

P. Bihari, M. Vippola, S. Schultes, M. Praetner, A.G. Khandoga, C.A. Reighel, C. Coester, T. Tuomi, M. Rehberg, F. Krombach. Optimized dispersion of nanopartciles for biological *in vitro* and *in vivo* studies. Part. Fibre Toxicol., (2008) 5, p. 14.

H.S. Choi, Y. Ashitate, J.H. Lee, S.H. Kim, A. Matsui, N. Insin, M.G. Bawendi, M. Semmler-Behnke, J.V. Frangioni, and A. Tsuda. Rapid translocation of nanoparticles from the lung airspaces to the body. Nat. Biotechnol., (2010) 28, pp. 1300–1303.

K. Donaldson, V. Stone, C.L. Tran, W. Kreyling, P.J.A. Borm. Nanotoxicology. Occup. Environ. Med., (2004) 61, pp. 727–728.

M. Ema, N. Kobayashi, M. Naya, S. Hanai, J. Nakanishi. Reproductive and developmental toxicity studies of manufactured nanomaterials. Reprod. Toxicol., (2010) 30, pp. 343–352.

European Commission. Commission recommendation of 18 October 2011 on the definition of nanomaterial. http://europa.eu/rapid/press-release_MEMO-11-704_en.htm Accessed August 3, 2012.

D. Hohr, Y. Steinfartz, R.P. Schins, A.M. Knaapen, G. Martra, B. Fubini, P.J. Borm. The surface area rather than the surface coating determines the acute inflammatory response after instillation of fine and ultrafine TiO_2 in the rat. Int. J. Hyg. Environ. Health, (2002) 205, pp. 239–244.

N. Kobayashi, M. Naya, S. Endoh, J. Maru, K. Yamamoto, J. Nakanishi. Comparative pulmonary toxicity study of nano-TiO_2 particles of different sizes and agglomerations in rats: different short- and long-term post-instillation results. Toxicology, (2009) 264, pp. 110–118.

W.G. Kreyling, M. Semmler, F. Erbe, P. Mayer, S. Takenaka, H. Schulz, G. Oberdörster, and A. Ziesenis, Translocation of ultrafine insoluble iridium particles from lung epithelium to extrapulmonary organs is size dependent but very low**.** J. Toxicol. Environ. Health A., (2002) 65, pp. 1513–1530.

J.G. Li, W.X. Li, J.Y. Xu, X.Q. Cai, R.L. Liu, Y.J. Li, Q.F. Zhao, Q.N. Li. Comparative study of pathological lesions induced by multiwalled carbon nanotubes in lungs of mice by intratracheal instillation and inhalation. Environ. Toxicol., (2007) 22, pp. 415–421.

G.Y. Liang, Y.P. Pu, L.H. Yin, R. Liu, B. Ye, Y.Y. Su, Y.F. Li. Influence of different sizes of titanium dioxide nanoparticle on hepatic and renal function in rats with correlation to oxidative stress. J. Toxicol. Environ. Health, (2009) 72, pp. 740–745.

T.F. Mar, G.A. Norris, J.Q. Koenig, T.V. Larson. Association between air pollution and mortality in Phoenix, 1995-1997. Environ. Health Perspect., (2000) 108, pp. 347–353.

A.D. Maynard, E.D. Kuempel. Airborne nanostructured particles and occupational health. J. Nanopart. Res., (2005) 7, pp. 587–614.

K.A. Miller, D.S. Siscovick, L. Sheppard, K. Shepherd, J.H. Sullivan, G.L. Anderson, J.D. Kaufman. Long-term exposure to air pollution and incidence of cardiovascular events in women. N. Engl. J. Med., (2007) 356, pp. 447–458.

N.L. Mills, H. Tornqvist, M.C. Gonzalez, E. Vink, S.D. Robinson, S. Söderberg, N.A. Boon, K. Donaldson, T. Sandström, A. Blomberg, D.E. Newby. Ischemic and thrombotic effects of dilute diesel-exhaust inhalation in men with coronary heart disease. N. Engl. J. Med., (2007) 357, pp. 1075–1082.

N.L. Mills, H. Törnqvist, S.D. Robinson, M.C. Gonzalez, S. Söderberg, T. Sandström, A. Blomberg, D.E. Newby, K. Donaldson. Air pollution and atherothrombosis. Inhal. Toxicol., (2007) 19, pp. 81–89.

Ministry of the Environment. http://www.env.go.jp/air/osen/pm/info.html

R.C. Murdock, L. Braydich-Stolle, A.M. Schrand, J.J. Schlager, S.M. Hussain. Characterization of nanomaterial dispersion in solusion prior to *in vitro* exposure using dynamic light scattering technique. Toxicol. Sci., (2008) 101, pp. 239–253.

J. Muller, M. Delos, N. Panin, V. Rabolli, F. Huaux, D. Lison. Absence of carcinogenic response to multiwall carbon nanotubes in a 2-year bioassay in the peritoneal cavity of the rat. Toxicol. Sci., (2009) 110, pp. 442–448.

A. Nel, T. Xia, L. Madler, N. Li. Toxic potential of materials at the nano level. Science, (2006) 311, pp. 622–627.

A.E. Nel, L. Mädler, D. Velegol, T. Xia, E.M. Hoek, P. Somasundaran, F. Klaessig, V. Castranova, M. Thompson. Understanding biophysicochemical interactions at the nanobio interface. Nat. Mater., (2009) 8, pp. 543–557.

A. Nemmar, P.H. Hoet, B. Vanquickenborne, D. Dinsdale, M. Thomeer, M.F. Hoylaerts, H. Vanbilloen, L. Mortelmans, B. Nemery. Passage of inhaled particles into the blood circulation in humans. Circulation, (2002) 105, pp. 411–414.

K. Noma, C. Goto, K. Nishioka, D. Jitsuiki, T. Umemura, K. Ueda, M. Kimura, K. Nakagawa, T. Oshima, K. Chayama, M. Yoshizumi, J.K. Liao, Y. Higashi. Roles of rho-associated kinase and oxidative stress in the pathogenesis of aortic stiffness. J. Am. Coll. Cardiol., (2007) 49, pp. 698–705.

G. Oberdörster, E. Oberdörster, and J. Oberdörster. Nanotoxicology: an emerging discipline evolving from studies of ultrafine particles. Environ. Health Perspect., (2005) 113, pp 823–839.

A. Peters, D.W. Dockery, J.E. Muller, M.A. Mittleman. Increased particle air pollution and the triggering of myocardial infarction. Circulation, (2001) 103, pp. 2810–2815.

T.M. Sager, D.W. Porter, V.A. Robinson, W.G. Lindsley, D.E. Schwegler-Berry, V. Castranova. Improved method to disperse nanoparticles for *in vitro* and *in vivo* investigation of toxicity. Nanotoxicology, (2007) 1, pp. 118–129.

T.M. Sager, C. Kommineni, V. Castranova. Pulmonary response to intratracheal instillation of ultrafine versus fine titanium dioxide: role of particle surface area. Part. Fibre Toxicol., (2008) 5, p. 17.

T.M. Sager, V. Castranova. Surface area of particle administered versus mass in determining the pulmonary toxicity of ultrafine and fine carbon black: comparison to ultrafine titanium dioxide. Part. Fibre Toxicol., (2009) 6, p. 15.

A. Seaton, W. MacNee, K. Donaldson, and D. Godden. Particulate air pollution and acute health effects. Lancet, (1995) 345, pp. 176–178.

A.A. Shvedova, E.R. Kisin, R. Mercer, A.R. Murray, J.V. Johnson, A.I. Potapovich, Y.Y. Tyurina, O. Gorelik, S. Arepalli, O. Schwegler-Berry, A.F. Hubbs, J. Antonini, D.E. Evans, B.K. Ku, D. Ramsey, A. Maynard, V.E. Kagan, V. Castranova, P.Baron. Unusual inflammatory and fibrogenic pulmonary responses to single-walled carbon nanotubes in mice. Am. J. Physiol. Lung. Cell. Mol. Physiol., (2005) 289, pp. 698–708.

J.S. Taurozzi, V.A. Hackley, M.R. Wiesner. Ultrasonic dispersion of nanoparticles for environmental, health and safety assessment—issures and recommendations. Nanotoxicology, (2011) 5, pp. 711–729.

Y. Taniyama, K.K. Griendling. Reactive oxygen species in the vasculature. Molecular and cellular mechanisms. Hypertension, (2003) 42, pp. 1075–1081.

The Royal Society & The Royal Academy of Engineering. Nanoscience and nanotechnologies:opportunities and uncertainties. Nanoscience and nanothechnologies, (2004).

J.S. Tsuji, A.D. Maynard, P.C. Howard, J.T. James, C.W. Lam, D.B. Warheit, A.B. Santamaria. Research strategies for safety evaluation of nanomaterials part IV: risk assessment of nanoparticles. Toxicol. Sci., (2006) 89, pp. 42–50.

D.B. Warheit, R.A. Hoke, C. Finlay, E.M. Donner, K.L. Reed, C.M. Sayes. Development of a base set of toxicity tests using ultrafine TiO_2 particles as a component of nanoparticle risk management. Toxicol. Lett., (2007) 171, pp. 99–110.

P. Wick, P. Manser, L.K. Limbach, U. Dattlaff-Weglikowska, F. Krumeich, S. Roth, W.J. Stark, A. Bruinink. The degree and kind of agglomeration affect carbon nanotube cytotoxicity. Toxicol. Lett., (2007) 168, pp. 121–131.

T. Xia, M. Kovochich, J. Brant, M. Hotze, J. Sempf, T. Oberley, C. Sioutas, J.I. Yeh, M.R. Wiesner, A.E. Nel. Comparison of the abilities of ambient and manufactured nanoparticles to induce cellular toxicity according to an oxidative stress paradigm. Nano Lett., (2006) 6, pp. 1794–1807.

S. Yamamoto, Ahmed S. Tin-Tin-Win-Shwe, T. Kobayashi, H. Fujimaki. Effect of ultrafine carbon black particles on lipoteichoic acid-induced early pulmonary inflammation in BALB/c mice. Toxicol. Appl. Pharmacol., (2006) 213, pp. 256–266.

2. Dispersion method for safety research on manufactured nanomaterials

2-1. Background

Recent studies have shown that exposure to various kinds of nanomaterials, such as metal oxide nanoparticles, carbon nanoparticles and nanotubes is injurious to biological systems (Wang et al., 2008, Kayat et al., 2011, Pauluhn., 2010, Tong et al., 2009, Johnston et al., 2009 and Cho et al., 2010). In addition to the gastrointestinal track and skin, the respiratory system is recognized as one of the most important portals of entry and target tissues, and a number of *in vivo* research studies have focused on the respiratory system to investigate the harmful effects of airborne nanomaterials (Oberdörster et al., 2005, Holsapple et al., 2005 and Krug et al., 2011). For the evaluation of respiratory toxicity, intratracheal instillation/spary and pharyngeal aspiration are useful and cost-effective exposure techniques routinely used in investigative exposure of animals to particles (Driscoll et al., 2000, Osier et al., 1997, Wallenborn et al., 2007, Shinohara et al., 2010, Warheit et al., 2007 and Porter et al., 2008). The dispersion medium (DM), an artificial physiological buffer comprised of protein and surfactant components naturally found in lung alveolar fluids, which are known to be effective in both reduction of agglomeration and stabilization of suspensions, was recommended in the preparation of nanomaterials suspension in pulmonary exposure studies using intratracheal instillation/spray or pharyngeal aspiration (Porter et al., 2008).

The aim of the present study was to investigate the factors that influence the dispersion status and establish a suitable and reproducible protocol for the preparation

of nanomaterial suspension specific for pulmonary exposure studies. Two kinds of different nanoparticles and one kind of carbon nanotube were dispersed in DM by direct probe-type sonicator or indirect cup-type sonicator. A series of sonication time and output power, as well as two different dispersion concentrations of particle suspension were tested. Size characterization was completed by dynamic light scattering (DLS) and further examined morphologically with transmission electron microscope (TEM). Dispersion stability over time was also assessed.

2-2. Methods

2-2-1 Nanomaterials

Titanium dioxide (TiO_2) nanoparticles (AEROXIDE TiO2 P25; Degussa AG, Dusseldorf, Germany) with primary diameter of 21 nm, zinc oxide (ZnO) nanoparticles (MKN-ZnO-020; mkNano, Missisauga, ONT, Canada) with primary diameter of 20 nm, and multi-walled carbon nanotube (MITSUI MWCNT-7; Mitsui, Tokyo, Japan) with diameter of 100 nm and length of 27 % >5 μm were used in the present study. The nanomaterials were stored in 50-ml polypropylene conical tubes until use.

2-2-2 Dispersion Medium (DM)

Porter et al. demonstrated that DM neither caused pulmonary inflammation or cytotoxicity, nor altered the toxicity of tested nanomaterials, suggesting that DM is an effective, biocompatible and economical vehicle for nanotoxicological evaluation. DM was prepared as described previously (Porter et al., 2008). Briefly, Ca^{2+} and Mg^{2+} -free

phosphate buffered saline (PBS) was supplemented with 5.5 mM D-glucose, 0.6 mg/ml bovine serum albumin (BSA), and 0.01 mg/ml 1,2-dipalmitoyl-sn-glycero-3-phosphocholine (DPPC), and sonicated for 10 min with continuous 70 W output power after mixing. DM was prepared within 2 days before dispersion and stored in a refrigerator at 4 ºC.

2-2-3 Suspension

Dispersion of nanomaterial suspension was performed in a 50-ml polypropylene conical tube. In terms of probe-type sonicator, we used the ultrasonic system (Sonifier 450 Advances; Branson, Danbury, CT) with a horn of which the tip diameter is 1/2" (13 mm). Particles were dispersed in 20 ml of DM and the tube was immersed in an ice-salt bath during sonication. As to the cup-type sonicator (cup horn; Branson), a circulatory cooling system was used to avoid over heating of the suspension. When the tube is immersed into the circulatory cooling bath, the maximum volume of suspension to be covered by cooling water is 8 ml, and therefore the volume of DM was adjusted to 8 ml. Output power was determined by the sonicator dial according to the manual provided by the manufacturer.

2-2-4 Size characterization

Soon after sonication, dispersed suspensions of 25 μg/ml TiO_2 nanoparticles (absorbance: 0.010; refractive index: 2.520) and 500 μg/ml ZnO nanoparticles (absorbance: 0.010; refractive index: 2.020) were prepared in DM (viscosity: 1.0; refractive index: 1.33), and then vortexed and filtered through a 0.6 μm isopore

membrane filter (Merk Millipore, Billerica, MA) into a disposable standard cuvette. Each sample was measured by dynamic light scattering (DLS) (Zetasizer Nano-S; Malvern Instruments, Worcestershire, UK) at 25 ºC four times after 1 hr on standing. Dispersion status was described as the peak value of the principal peak of the intensity-weighted hydrodynamic diameter distribution (peak 1), in conjunction with polydispersity index (PdI), which reflected the broadness of the size distribution (scale range from 0 to 1, with 0 being monodispersion and 1 being polydispersion) (Murdock et al., 2008).

To check the stability of suspension, size characterization was conducted soon after, and at 1, 3, and 7 days post-sonication (ZnO nanoparticles was not measured at 3 days post-sonication because of inadequacy of samples). The prepared dispersions were stored in a refrigerator at 4ºC until measured, and after vortexing for several seconds they were subsequently analyzed at DLS as mentioned previously.

2-1-5 Morphological characterization

A drop (approximately 0.1 ml) of each sample was deposited onto an elastic carbon-coated copper grid or high-resolution carbon-coated copper grid to observe the dispersed TiO_2 nanoparticles or MWCNT, respectively, and allowed to air dry. A transmission electron microscope (TEM, JEM-1011; JEOL, Tokyo) was used to visualize the dispersed nanomaterials. MWCNTs suspension was also viewed using an Olympus BXJ1 optical microscope (OLYMPUS, Tokyo) equipped with a digital camera DP70, to capture images with the DP controller software (OLYMPUS).

2-3. Results

2-3-1 Direct probe-type sonicator

2-3-1.1 Particle concentration for DLS measurement

Suspensions of TiO_2 and ZnO nanoparticles at concentration of 0.5 mg/ml were dispersed by probe-type sonicator at 20 W, 80 % pulse mode, for 5, 10, 20, or 30 min. The sample dispersed for 30 min was diluted with DM into concentrations of 10, 25, 50, 100, 200, and 500 μg/ml, and peak1 and PdI values were determined for each concentration sample (Fig. 1).

TiO_2 nanoparticles showed the smallest peak1 and PdI at the concentration of 25 μg/ml. At particle concentrations ranging from 25 to 500 μg/ml, the secondary hydrodynamic diameter increased with elevated concentration. The coefficient of variation of peak1 was 12.63, 5.18, 19.26, 25.50, 42.24 and 34.82 % at concentrations of 10, 25, 50, 100, 200 and 500 μg/ml, respectively, indicating the least deviation of size distribution at the concentration of 25 μg/ml.

On the contrary, peak 1 and its standard deviation of ZnO nanoparticles slightly decreased with elevated particle concentration, and PdI of ZnO nanoparticles also decreased depending on the particle concentration to a greater extent than the peak 1 of ZnO nanoparticles. The size distribution provided by DLS (Fig. 2) showed unimodal distribution at the concentration of 500 μg/ml, while there was a small sub-peak around 8 nm at 100 μg/ml. The size distribution of DM was measured to confirm that the peak around 8 nm was derived from DM.

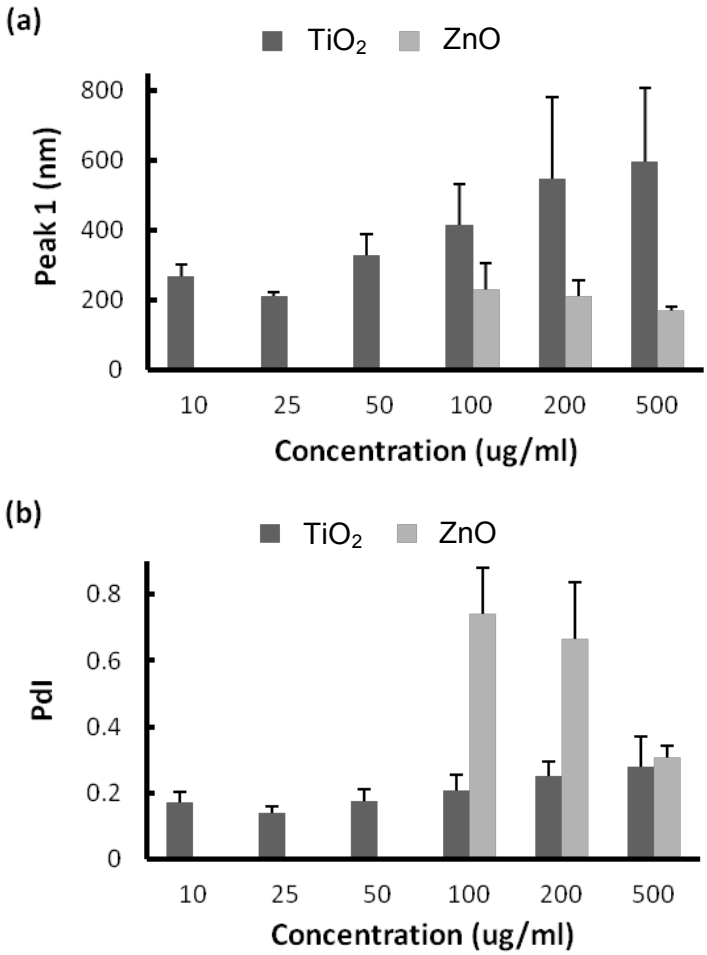

Fig. 1. Size characterization at concentrations of 10, 25, 50, 100, 200, and 500 μg/ml of TiO_2 or ZnO nanoparticle suspensions dispersed by a probe-type sonicator at 20 W, 80 % pulse mode, for 30 min: (a) peak 1 and (b) PdI. Data are mean ± SD.

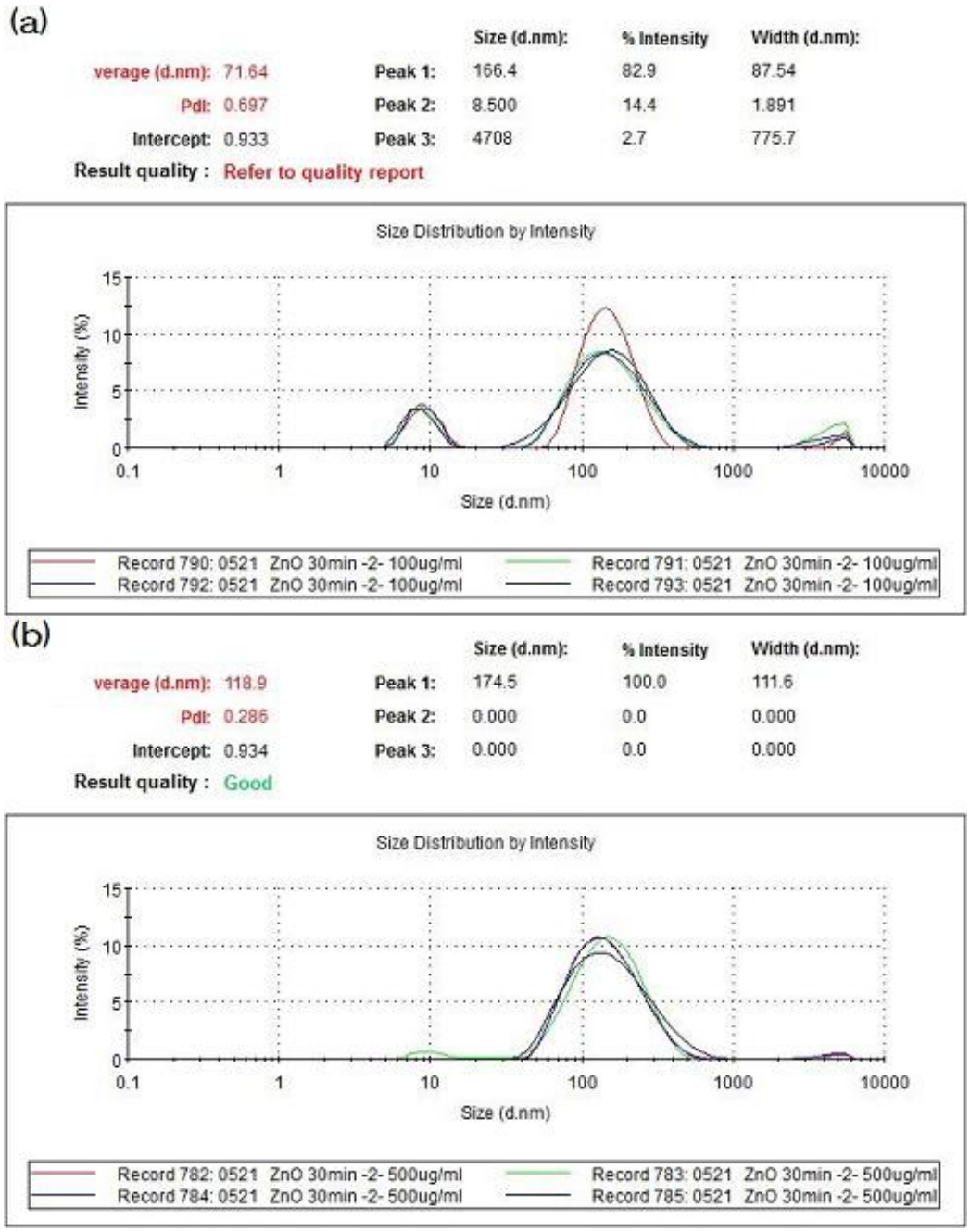

Fig. 2. Report of size distribution of ZnO nanoparticles suspensions dispersed by a probe-type sonicator at 20 W, 80 % pulse mode, for 30 min, at concentrations of: (a) 100 and (b) 500 μg/ml.

2-3-1.2 Dispersion time

Suspensions of TiO_2 and ZnO nanoparticles at concentration of 0.5 mg/ml were at dispersed by probe-type sonicator 20 W, 80 % pulse mode, for 5, 10, 20, or 30 min. With increased dispersion time, DLS measurement showed a decrease in hydrodynamic diameter of both TiO_2 and ZnO nanoparticles, as well as tendency toward monodispersion of TiO_2 nanoparticles and decreased standard deviation of PdI of ZnO nanoparticles (Fig. 3).

TEM showed the presence of smaller TiO_2 nanoparticle agglomerates in 30-min sonicated samples (Fig. 4 (b)) compared with the large agglomerates found after sonication for 10 min (Fig. 4 (a)).

These results suggest that longer dispersion time allowed the delivery of more energy to break the bonds within the agglomerates. After filtration, poor dispersion suspension (5 or 10 min) appeared more limpid, probably due to the retention of larger number of micro-sized agglomerates on the filter membrane. In comparison, samples sonicated for 30 min appeared turbid and this indicated that the majority of small agglomerates distributed well in the dispersed suspension (Fig. 5).

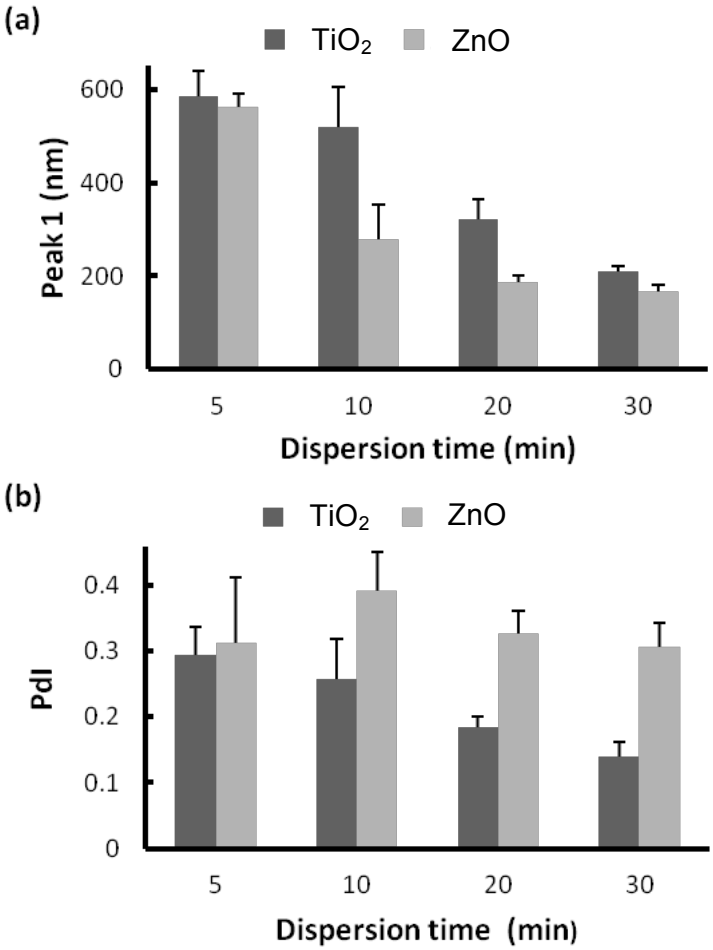

Fig. 3. Size characterization of TiO_2 and ZnO nanoparticle suspensions at concentration of 0.5 mg/ml dispersed by a probe-type sonicator at 20 W, 80 % pulse mode for, 5, 10, 20, or 30 min: (a) peak 1 and (b) PdI. Data are mean ± SD.

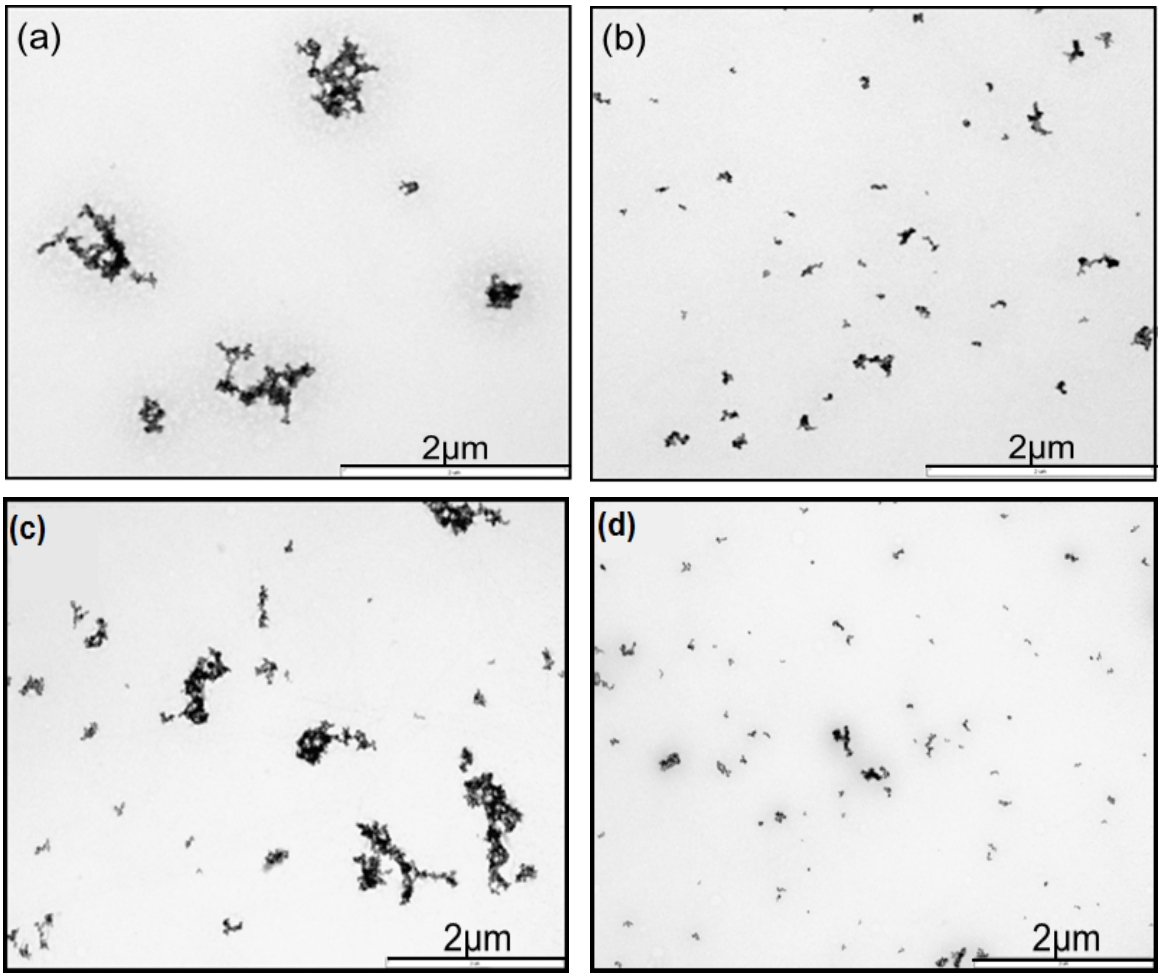

Fig. 4. TEM micrographs of TiO_2 nanoparticle suspensions at concentration of 0.5 mg/ml dispersed by (A) a probe-type sonicator at 20 W, 80 % pulse mode, for (a) 10 min and (b) 30 min; (B) a cup-type sonicator at (c) 50 W and (d) 100W, 80 % pulse mode, for 10 min.

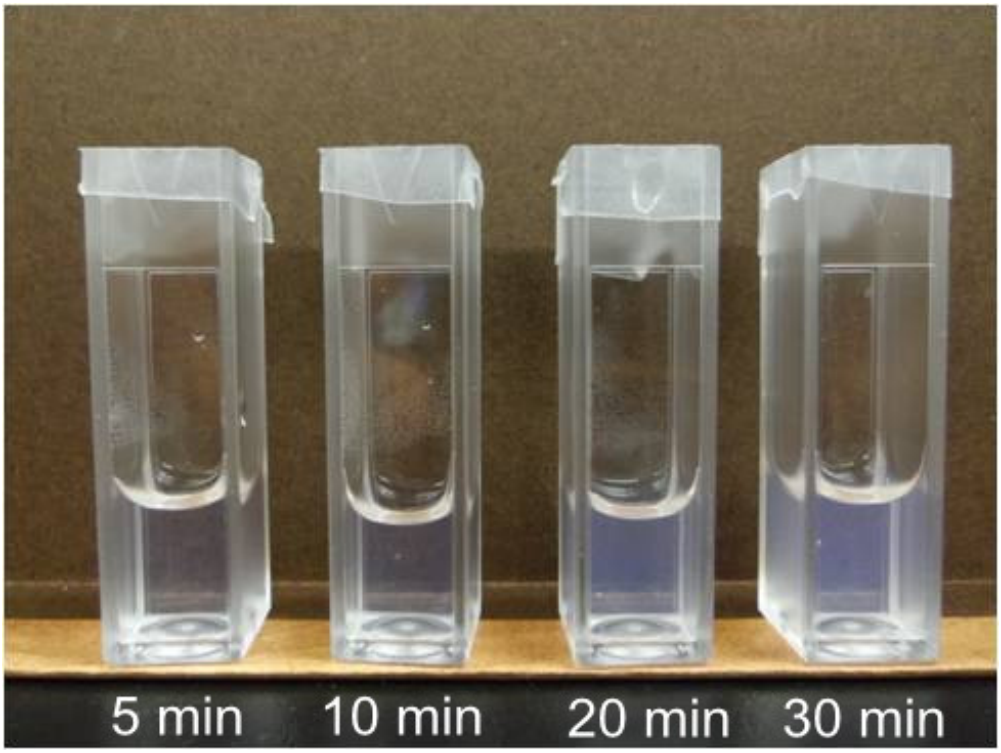

Fig. 5. Change in the turbidity of filtered TiO_2 nanoparticle suspensions dispersed by a probe-type sonicator at 20 W, 80 % pulse mode, for 5, 10, 20, or 30 min at concentration of 0.5 mg/ml.

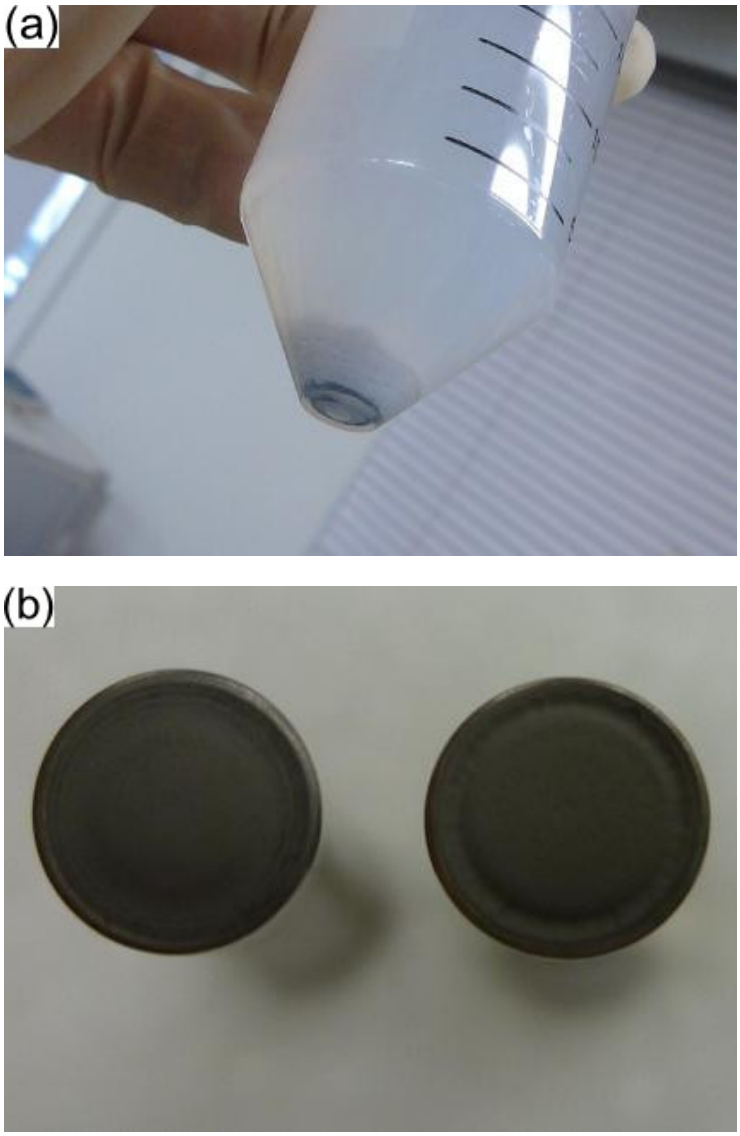

Fig. 6. (a) Black sediment at the bottom of a sample sonicated by a probe-type sonicator at 20 W, 80% pulse mode, for 30 min after 2 hours on standing and (b) the tip surface of unused probe (left) and abrased probe (right).

2-3-1.3 Contamination from the probe

Black sediment was found at the bottom of the samples sonicated for 30 min after 2 h on standing (Fig. 6 (a)). Inspection of the surface of the probe tip showed abrasion, which was probably due to the intense cavitation (Fig. 6 (b)). These microscopic tip residues of titanium were presumed to be broken away from the tip into the suspension.

2-3-2 Indirect cup-type sonicator

2-3-2.1 Temperature of cooling water

Suspensions of TiO_2 nanoparticles at concentration of 0.5 mg/ml were dispersed by cup-type sonicator at 220 W (max), 80 % pulse mode. For the purpose of suppression of sample heating, a circulatory cooling system consisting of a congealer that circulated 30 % ethanol with a pump at the flow rate of 400 ml/min was utilized. At the beginning, we attempted to lower the temperature of cooling water to −10 °C so that sonication was able to be carried out with long dispersion time. When sonicated for 40 min, agglomerated TiO_2 nanoparticles were dispersed into 371.8 ± 12.5 nm with PdI of 0.24 ± 0.01 when the circulation temperature was set at −10 °C, and the sample temperature was measured lower than the room temperature (25 °C) after dispersion. In contrast, when the circulation temperature was set at 5°C, particles were dispersed into 173.9 ± 12.8 nm with PdI of 0.15 ± 0.01 after 10-minute sonication, and the sample was heated to 37.6 °C. In spite of the shorter dispersion time, sonication at a relatively higher temperature (5 °C) produced better monodispersion of small agglomerates, suggesting that the cup-type sonication system should be cooled to

moderate temperatures only. Since the sample was extremely calefacient at dispersion time longer than 10 min, we chose a dispersion time of 10 min for the suspension using the cup-type sonicator.

2-3-2.2 Output power of sonicator

Suspensions of TiO_2 and ZnO nanoparticles at concentration of 0.5 mg/ml were dispersed by the cup-type sonicator at 10, 20, 50, 100, or 220 W, 80 % pulse mode, for 10 min (Fig. 7). The size of the sonicated TiO_2 nanoparticles appeared to decrease with increased output power, although the maximum reduction reached a plateau level at output power of 100 W, and a similar trend was noted for PdI. More energy delivered with higher output power facilitated disruption of agglomeration and output power of 100 W was deemed likely to be adequate for dispersion of TiO_2 nanoparticles. TEM micrographs of the samples sonicated at 50 or 100 W confirmed the results of DLS (Fig. 4).

Surprisingly, output power ranging from 10 to 220 W had little effect on sizes of agglomerated ZnO nanoparticles, while PdI showed an output power-dependent decrease from 10 to 50 W. The energy delivered with output power of 10 W might be enough for agglomerate breakage, but output power less than 50 W was insufficient to accomplish monodispersion.

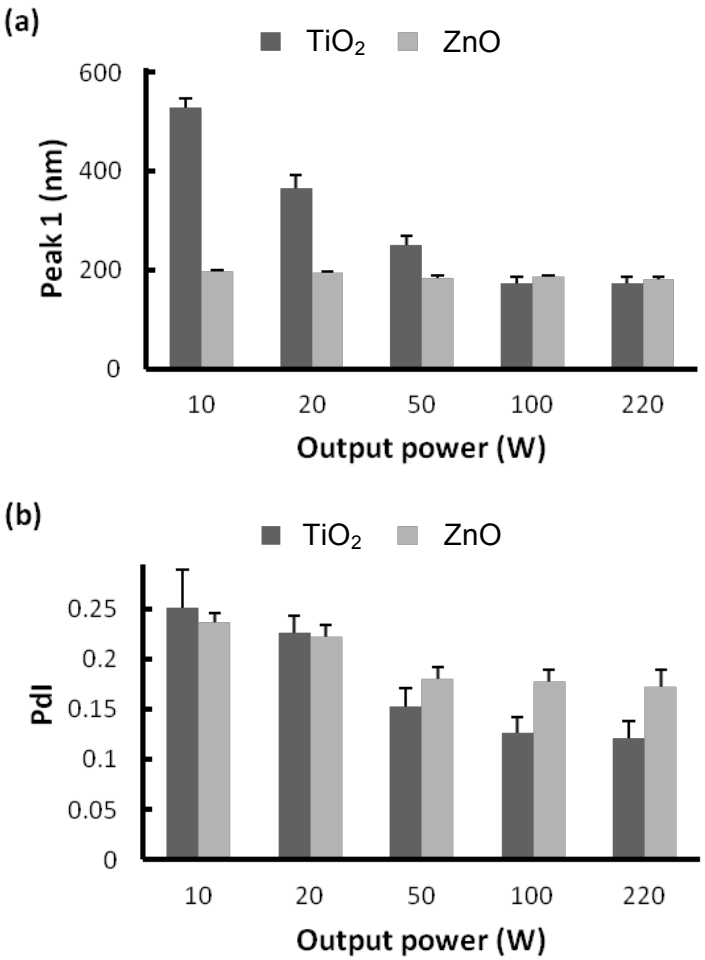

Fig. 7. Size characterization of TiO_2 and ZnO nanoparticle suspensions at concentration of 0.5 mg/ml dispersed by a cup-type sonicator at 10, 20, 50, 100, or 220 W, 80 % pulse mode, for 10 min: (a) peak 1 and (b) PdI. Data are mean ± SD.

2-3-2.3 Determination of dispersion time

We also compared the size distribution between samples sonicated at 220 W, 80 % pulse mode for 10 min and that of samples sonicated several times each for 10 min, with sample cooling in between the sonications. The size of agglomerated TiO_2 nanoparticles sonicated four times each for 10 min was 182.2 ± 0.6 nm, which was similar to 173.9 ± 12.8 nm obtained after a single sonication. Regarding to ZnO nanoparticles, one single sonication for 10 min dispersed the agglomerates into 180.2 ± 5.0 nm and three-time sonication also yielded similar result as 177.5 ± 1.5 nm. This phenomenon was speculated to be the result of the balance of deagglomeration and reagglomeration taking place within the process of increasing delivered energy (Taurozzi et al., 2011). It seemed that sonication at 220 W, 80 % pulse mode, for 10 min was favorable for the dispersion of these two nanoparticles.

2-3-3 Applicability

2-3-3.1 Particle concentration for dispersion

Suspensions of TiO_2 and ZnO nanoparticles at concentrations of 0.5 or 2.5 mg/ml were dispersed by the cup-type sonicator at 220 W, 80 % pulse mode, for 10 min. At the concentration of 2.5 mg/ml, TiO_2 nanoparticles agglomerated to a slightly larger size with larger standard deviation, while significant reduction of the secondary diameter of ZnO nanoparticles was found with comparison to the outcome of 0.5 mg/ml samples (Table 1).

Table 1. Effect of particle concentration for dispersion.

	Concentration (mg/ml)			
	0.5		2.5	
Nanoparticle	Peak 1 (nm)	PdI	Peak 1 (nm)	PdI
TiO_2	173.9 ± 12.8	0.12 ±0.02	180.8 ±31.4	0.13 ±0.02
ZnO	180.2 ± 5.0	0.18 ± 0.01	169.8 ± 3.1*	0.17 ± 0.02

Data are mean ± SD; * $p < 0.05$.

2-3-3.2 Stability of suspension

Suspensions of TiO_2 and ZnO nanoparticles at concentration of 0.5 mg/ml were dispersed by a cup-type sonicator at 100 or 220 W, 80 % pulse mode, for 10 min. The size distributions conducted soon after, and at 1, 3, and 7 days post-sonication are listed in Table 2. The secondary diameter of TiO_2 nanoparticle agglomerates increased by 4.7 %, 7.8 % and 9.2 % when dispersed at 100 W, and by 1.5 %, 5.9 % and 4.5 % at 220 W, respectively. As to ZnO nanoparticles, the secondary diameter increased by 1.9 % and 3.4 % (1 and 7 days post-sonication, respectively) at 100 W, and by 1.3 % and 0.6 % at 220 W.

Table 2. Stability of nanoparticle suspensions.

Particles	Output power	Peak 1 (nm)			
		0 day	1 day	3 days	7 days
TiO_2	100 W	174.0 ± 12.3	182.1 ± 14.6	187.5 ± 19.2	190.0 ± 20.6
	220 W	173.9 ± 12.8	176.5 ± 13.6	184.1 ± 11.8	181.7 ± 16.2
ZnO	100 W	177.2 ± 4.7	180.6 ± 4.7	-	183.3 ± 4.9
	220 W	180.2 ± 5.0	182.5 ± 4.1	-	179.2 ± 4.5

Data are mean ± SD.

2-3-3.3 Dispersion of MWCNTs

Dispersion of suspensions of MWCNTs at a concentration of 2.0 mg/ml was operated using the protocol: cup-type sonicator at 100 W, 80 % pulse mode, for 10 min. The dispersion status was assessed using optical microscopy and TEM. Highly agglomerated masses of MWCNTs were dispersed into smaller size clusters after a single dispersion process (Fig. 8 (a) and (b)) and MWCNTs bundles were separated homogeneously by sonication for another 10 min (Fig. 8 (c)). Individual and bundled nanotubes were observed in samples sonicated twice in the TEM micrographs (Fig. 8 (d)).

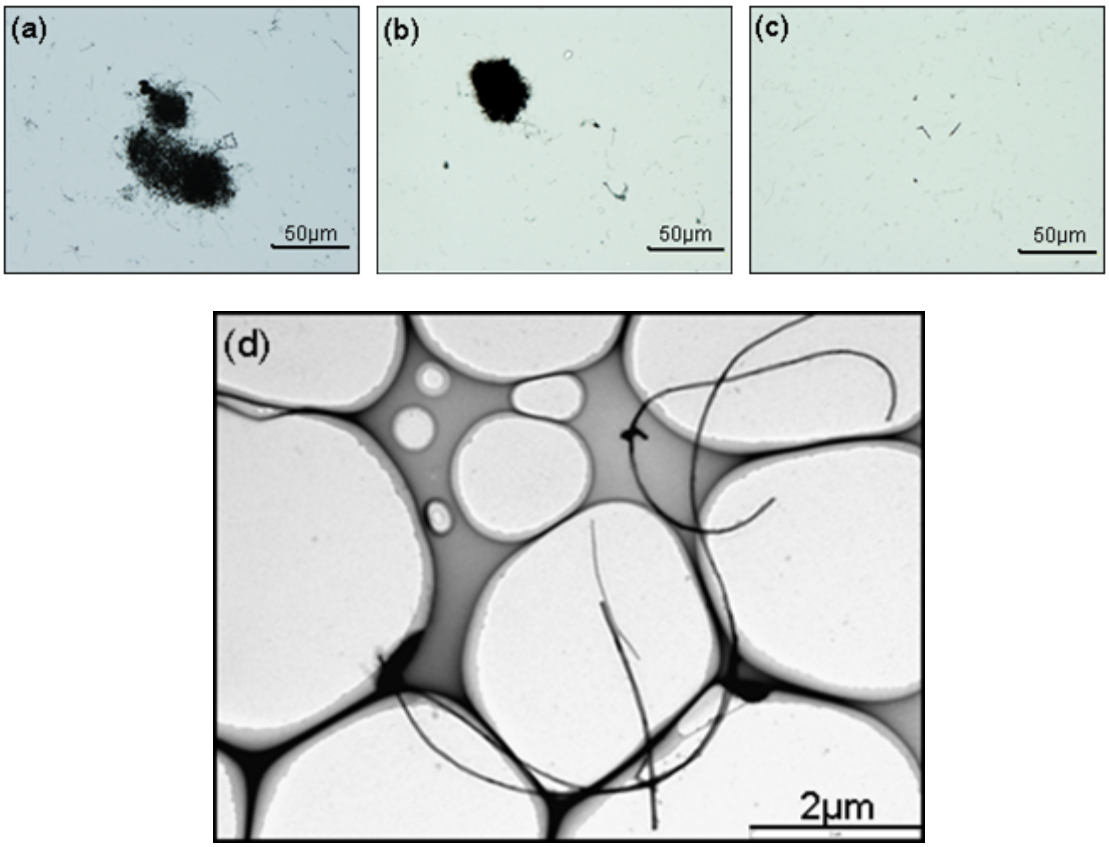

Fig. 8. Optical microscope micrographs of MWCNT suspensions at concentration of 2.0 mg/ml: (a) un-dispersed, (b) dispersed by a cup-type sonicator at 100 W, 80 % pulse mode, for 10 min, and (c) for another 10 min; and (d) TEM micrograph of MWCNT sonicated twice.

2-4 Summary

The present study used direct probe-type and indirect cup-type sonicator to prepare nanomaterials suspensions and subsequent size characterization was compeleted by DLS instrument and TEM. The effects of factors including particle concentration, dispersion time and output power of sonication on the dispersion status were investigated. Then a protocol was established and demonstrated to be suitable and reproducible for nanomaterials dispersion in terms of both size distribution and suspension stability.

2-5 References

W.S. Cho, R. Duffin, C.A. Poland, S.E.M. Howie, W. MacNee, M. Bradley, I.L. Megson, K. Donaldson. Metal oxide nanoparticles induce unique inflammatory footprints in the lung: important implications for nanoparticle testing. Environ. Health Perspect., (2010) 118, pp. 1699–1706.

K.E. Driscoll, D.L. Costa, G. Hatch, R. Henderson, G. Oberdorster, H. Salem, R.B. Schlesinger. Intratracheal instillation as exposure technique for the evaluation of respiratory track toxicity: uses and limitaitons. Toxicol. Sci., (2000) 55, pp. 24–35.

M.P. Holsapple, W.H. Farland, T.D. Landry, N.A. Monteiro-Riviere, J.M. Carter, N.J. Walker, K.V. Thomas. Research strategies for safety evaluation of nanomaterials, part II: toxicological and safety evaluation of nanomaterials, current challenges and data needs. Toxicol. Sci., (2005) 88, pp. 12–17.

H.J. Johnston, G.R. Hutchison, F.M. Christensen, S. Peters, S. Hankin, V. Stone. Identification of the mechanisms that drive the toxicity of TiO_2 particulates: the contribution of physicochemical characteristics. Part. Fibre Toxicol., (2009) 6, p. 33.

J. Kayat, V. Gajbhiye, R.K. Tekade, N.K. Jain. Pulmonary toxicity of carbon nanotubes: a systematic report. Nanomedicine, (2011) 7, pp. 40–49.

H.F. Krug, P. Wick. Nanotoxicology: an interdisciplinary challenge. Angew. Chem. Int. Ed., (2011) 50, pp. 1269–1278.

R.C. Murdock, L. Braydich-Stolle, A.M. Schrand, J.J. Schlager, S.M. Hussain. Characterization of nanomaterial dispersion in solution prior to *in vitro* exposure using dynamic light scattering technique. Toxicol. Sci., (2008) 101, pp. 239–253.

G. Oberdörster, E. Oberdörster, J. Oberdörster. Nanotoxicology: an emerging discipline evolving from studies of ultrafine particles. Environ. Health Perspect., (2005) 113, pp. 823–839.

M. Osier, R.B. Baggs, G. Oberdorster. Intratracheal instillation versus intratracheal inhalation: influence of cytokines on inflammatory response. Environ. Health Perspect., (1997) 105, pp. 1265–1271.

J. Pauluhn. Multi-walled carbon nanotubes: approach for derivation of occupational exposure limit. Regul. Toxicol. Pharmacol., (2010) 57, pp. 78–89.

D. Porter, K. Sriram, M. Wolfarth, A. Jefferson, D. Schwegler-Berry, M. Andrew, V. Castranova. A biocompatible medium for nanoparticle dispersion. Nanotoxicology, (2008) 2, pp. 144–154.

T.M. Sager, V. Castranova. Surface area of particle administered versus mass in determining the pulmonary toxicity of ultrafine and fine carbon black: comparison to ultrafine titanium dioxide. Part. Fibre Toxicol., (2009) 6, p. 15.

N. Shinohara, T. Nakazato, M. Tamura, S. Endoh, H. Fukui, Y. Morimoto, T. Myojo, M. Shimada, K. Yamamoto, H. Tao, Y. Yoshida, J. Nakanishi. Clearance kinetics of fullerene C_{60} nanoparticles from rat lungs after intratracheal C_{60} instillation an inhalation C_{60} exposure. Toxicol. Sci., (2010) 118, pp. 564–573.

A.A. Shvedova, E.R. Kisin, R. Mercer, A.R. Murray, J.V. Johnson, A.I. Potapovich, Y.Y. Tyurina, O. Gorelik, S. Arepalli, O. Schwegler-Berry, A.F. Hubbs, J. Antonini, D.E. Evans, B.K. Ku, D. Ramsey, A. Maynard, V.E. Kagan, V. Castranova, P. Baron. Unusual inflammatory and fibrogenic pulmonary responses to single-walled carbon nanotubes in mice. Am. J. Physiol. Lung. Cell. Mol. Physiol., (2005) 289, pp. 698–708.

J.S. Taurozzi, V.A. Hackley, M.R. Wiesner. Ultrasonic dispersion of nanoparticles for environmental, health and safety assessment—issures and recommendations. Nanotoxicology, (2011) 5, pp. 711–729.

H. Tong, J.K. McGee, R.K. Saxena, U.P. Kodavanti, R.B. Devlin, M.I. Gilmour. Influence of acid functionalization on the cardiopulmonary toxicity of carbon nanotubes and carbon black particles in mice. Toxicol. Appl. Pharmacol., (2009) 239, pp. 224–232.

J.G. Wallenborn, J.K. McGee, M.C. Schladweiler, A.D. Ledbetter, U.P. Kodavanti. Systemic translocation of particulate matter-associated metals following a single intratracheal instillation in rats. Toxicol. Sci., (2007) 98, pp. 231–239.

D.B. Warheit, T.R. Webb, K.L. Reed, S. Frerichs, C.M. Sayes. Pulmonary toxicity study in rats with three forms of ultrafine-TiO_2 particles: differential responses related to surface properties. Toxicology, (2007) 230, pp. 90–104.

3. Zinc oxide nanoparticles induce migration and adhesion of monocytes to endothelial cells and accelerate foam cell formation

3-1 Background

TiO_2 and zinc oxide (ZnO) nanoparticles are widely used in paints, pharmaceutical, and cosmetic industries. The rapidly developing field of nanotechnology becomes a source for human potential exposures to engineered nanoparticles by different routes: inhalation (respiratory tract), ingestion (gastrointestinal tract), dermal (skin), and injection (blood circulation) (Oberdörster et al., 2005).

Atherosclerosis is a disease of the vasculature characterized by a chronic inflammation of the arterial wall and the formation of fibrotic plaques in the major arteries (Lusis., 2000). The process of atherosclerogenesis is initiated by the activation of endothelial cells, with subsequent migration of mononuclear cells and expression of adhesion molecules for inflammatory cells (Berk., 2008 and Libby et al., 2009). In addition, a critical factor in the progression of atherosclerogenesis is the development of an oxidizing environment caused by the activation of macrophages that become loaded with oxidized low-density lipoprotein (LDL) and other lipids (Tsimikas and Miller, 2001). The formation of foam cells is crucial in the initiation and progression of atherosclerosis, and one of the critical steps in foam cell formation is the uptake of modified LDL by macrophages via scavenger receptors (Moore and Freeman, 2006).

The present study investigated the effects of nanosized metal oxide particles on the migration and adhesion of monocytes, which are essential processes in atherosclerogenesis, using an in vitro set-up of human umbilical vein endothelial cells

(HUVECs) and human monocytic leukemia cells (THP-1). We also examined the effects of exposure to nanosized metal oxide particles on macrophage cholesterol uptake and foam cell formation.

3-2 Methods

3-2-1 Nanoparticle preparation and characterization

TiO_2 nanoparticles (AEROXIDE TiO_2 P25; Degussa AG, Dusseldorf, Germany) with a primary diameter of 21 nm, and ZnO nanoparticles (MKN-ZnO-020; mkNANO, Mississauga, ONT, Canada) with a primary diameter of 20 nm were used in the present study. Nanoparticles were suspended in culture media and dispersed using sonicator (BRANSON Sonifier model 450, Danbury, CT, 80 % pulsed mode, 100 W, 15 min), as described previously (Wu et al., 2013). The hydrodynamic sizes of the particles in media were measured four times after 1 hr on standing using the dynamic light scattering (DLS) technology with a Zetasizer Nano-S (Malvern Instruments, Worcestershire, UK). Dispersion status was described by the intensity-weighted hydrodynamic average diameter (z-average) and polydispersity index (PdI), which reflect the broadness of the size distribution (scale range from 0 to 1, with 0 being monodispersion and 1 being polydispersion) (Murdock et al., 2008).

2-2-2 Cell culture

HUVECs from Lonza Group (Basel, Switzerland) were cultured in endothelial basal medium-2 containing endothelial growth media supplement bullet kit (Lonza Group)

at 37 °C in 5 % CO_2. Cells were passaged with trypsin-EDTA, trypsin neutralizing solution and HEPES buffering solution (Lonza Group) every 2–3 days and experiments were performed between passages 3 and 4. THP-1 cells from the American Type Culture Collection (ATCC) (Rockville, MD) were cultured in RPMI 1640 medium (Invitrogen, Grand Island, NY) containing 10 % FBS with penicillin (100 U/ml) and streptomycin (100 μg/ml) at 37 °C in 5 % CO_2. For the differentiation of THP-1 monocytes into macrophage-like cells, THP-1 cells were treated with 162 nM 12-myristate 13-acetate (PMA) (Sigma-Aldrich, St Louis, MO) for 16 hr in RPMI 1640 medium containing 10 % FBS.

3-2-3 Cell viability assay

HUVECs were seeded at 1.5×10^4 cells per well on 96-well plates overnight prior to the experiment. Nanoparticles were dispersed in complete medium, the final concentrations of nanoparticles ranged from 1 to 100 μg/ml. Cell viability was determined after incubation of suspended nanoparticles for 24 hr by MTS assay as indicated by the CellTiter 96 AQueous One Solution (Promega, Madison, WI), which measures mitochondrial function and correlates with cell viability. After exposure, the cells were incubated with fresh medium (phenol red-free) containing MTS reagent for 1 hr before absorbance measurements at 490 nm. The effect of nanoparticles on cell proliferation was calculated as the percentage of inhibition of cell growth with respect to the controls. THP-1 monocytes were seeded at 1.5×10^4 cells per well on 96-well plates, exposed to nanoparticles at a concentration ranging from 1 to 100 μg/ml for 3

hr, and then treated with 162 nM PMA for 16 hr in RPMI 1640 medium containing 10 % FBS. Cell viability was determined by MTS as described above.

3-2-4 Inductively coupled plasma mass spectrometry

To evaluate the uptake of nanoparticles by the cells using inductively coupled plasma mass spectrometry (ICP-MS), confluent HUVECs in 150 mm dishes were exposed to 1, 5 and 10 μg/ml of TiO_2 or ZnO particles. After 16 hr, cells were washed with Hanks' Balanced Salt Solution (HBSS; Invitrogen), detached using trypsin, and harvested with complete cell culture media. The cell suspensions were centrifuged at 200 × g for 3 min at 4 °C. The cell pellet was suspended in 1 ml of HBSS, and the number of cells was calculated. The solutions were mixed with concentrated nitric acid (HNO_3; Wako, Osaka, Japan) to reach the final HNO_3 concentration of 3 %, and then heated to 80 °C until cell content was dissolved, as described previously (Gojova et al., 2007). A blank control solution was prepared for ICP-MS reaction (without cells) by mixing 1 of the HBSS with the same amount of concentrated HNO_3; this solution was processed the same way as the sample solutions. Finally, the dissolved solutions were adjusted to a volume of 10 ml with 3 % HNO_3 in water and used for ICP-MS analysis. The concentrations of Ti and Zn were determined using Agilent ICP-MS 7700 (Agilent Technologies, Santa Clara, CA).

3-2-5 Detection of intracellular free zinc ion

Intracellular free zinc ion was visualized using a fluorescent, membrane permeable probe Zinquin ethyl ester (Dojindo, Kumamoto, Japan) as described previously (Zalewski et al., 1994). Briefly, HUVECs (1×10^5 cells/ml) were seeded on 24-well plates. After 16 hr, cells were exposed to 10 μg/ml of TiO_2 or ZnO for 16 hr. After washing with HBSS three times, the cells were treated with 25 μM of Zinquin ethyl ester for another 30 min at 37 °C. Cells were washed with HBSS and observed using a fluorescent microscope; FSX100 (Olympus, Tokyo, Japan).

3-2-6 Monocyte chemotaxis assay

HUVECs (1×10^5 cells/ml) were seeded on 24-well plates and allowed to adhere to the plate for overnight. HUVECs were exposed to TiO_2 or ZnO (both at 1, 5, 10 μg/ml) particles for 16 hr, centrifuged (10,000 × g, 10 min) to remove any suspended nanoparticles, and then the supernatant was obtained. The supernatants were harvested and used as the chemoattractant in the lower chamber of Cell Culture inserts (8.0 mm pore size, 24-well plates; BD Falcon, Franklin, NJ), as described previously (Shaw et al., 2011) with minor modification. THP-1 cells were loaded into the upper chamber (n = 3, 2.5×10^5 cells/well) and incubated for 2 hr at 37 °C (Fig. 1A). Cells that had actively migrated through the membrane were fixed (100 % ethanol; 5 min) and stained with crystal violet (Sigma Aldrich). Transmigration was quantified by counting the number of cells present in four randomly selected fields using a light microscope at a magnification of × 200. After exposure of HUVECs to different doses (1, 5, or 10 μg/ml) of TiO_2 or ZnO particles for 16 hr at 37 °C, monocyte chemotactic

protein-1 (MCP-1) levels were measured using ELISA (eBioscience, San Diego, CA) according to the protocol supplied by the manufacturer.

3-2-7 Cell adhesion assay

The adhesion of THP-1 cells to HUVECs was assessed as described previously (Choi et al., 2003) with minor modifications. HUVECs (1.5×10^4 cells) were grown overnight in 96-well plates at 37 °C. The cells were exposed to different doses (1, 5, or 10 μg/ml) of TiO_2 or ZnO particles for 16 hr at 37 °C and prior to the adhesion assay, washed three times with HBSS containing 0.1 % BSA. THP-1 cells were suspended at a density of 1.0×10^6 cells/ml of 0.1 % BSA/HBSS and labeled with 1 μM of calcein-AM (BD Bioscience, Franklin Lakes, NJ) by 30 min incubation at 37 °C, followed by three washings with 0.1% BSA/HBSS. Labeled THP-1 cells were then incubated with HUVECs exposed to nanoparticles for 30 min at 37 °C. Nonadherent cells were removed by careful three-time washings with 0.1 % BSA/HBSS. The adherence of calcein-labeled THP-1 cells was quantified by counting the number of endothelial monolayers using a fluorescent microscope; FSX100.

For western blot analysis, HUVECs were lysed in radioimmunoprecipitation assay (RIPA) lysis buffer containing protease inhibitors (Santa Cruz, Dallas, TX). The concentration of extracted protein was measured in triplicate using the Protein Assay Dye Reagent Concentrate (Bio-Rad Laboratories, Hercules, CA). Protein samples (n = 3 or 4 in each group) were separated by 12 % SDS-PAGE and transferred onto polyvinylidene difluoride (PVDF) membranes (Immobilon-P, Millipore, Billerica, MA). The membranes were incubated with a rabbit monoclonal antibody to

intracellular adhesion molecule-1 (ICAM-1) (Abcam, Cambridge, MA) at a dilution of 1:500 and a mouse monoclonal antibody to vascular cell adhesion molecule-1 (VCAM-1) (Abcam) at a dilution of 1:500. Mouse anti-β-actin (ACTB) monoclonal antibody (Sigma-Aldrich) at dilution 1:5000 was used as a loading control. Immunoreactive bands were visualized using ECL-select chemiluminescence reagent (GE Healthcare—Amersham, Buckinghamshire, UK) and the intensity of the bands was quantified by Quantity One v3.0 software (Bio-Rad Laboratories). Protein expression levels were normalized relative to the level of β-actin protein in the same sample.

3-2-8 DiI-acetylated-LDL uptake assays

THP-1 cells (3×10^5 cells) were seeded on 24-well plates, exposed to the suspended nanoparticles for 3 h, and then treated with 162 nM PMA for 16 hr in RPMI 1640 medium containing 10 % FBS. The adherent cells were used as monocyte/macrophages for acetylated-LDL (Ac-LDL) uptake assay. The differentiated THP-1 cells were incubated at 37 °C with 10 μg/ml of 1,1′-dioctadecyl-3,3,3′,3′-tetramethylin docarbocyaninet (DiI)-AcLDL (Life Science Technologies, Carlsbad, CA) in RPMI-1640 containing 0.2 % (v/v) fatty acid-free BSA for 6 hr as described previously (McLaren et al., 2010 and Oh et al., 2012). DiI-AcLDL uptake was analyzed by flow cytometry on a FACS Canto II (BD Biosciences) flow cytometer with at least 10,000 events acquired for each sample. DiI-AcLDL uptake is represented as a percentage with the untreated control indicated as 100 %.

3-2-9 Oil Red O staining

To investigate foam cell formation, THP-1 cells (2×10^5 cells) were seeded on Culture Slides (8-well, BD Biosciences), exposed to the suspended nanoparticles for 3 hr, and then treated with 162 nM PMA for 16 hr in RPMI 1640 medium containing 10 % FBS. The differentiated THP-1 cells were incubated at 37 °C with 10 μg/ml of Ac-LDL (Life Science Technologies) in RPMI-1640 containing 0.2 % (v/v) fatty acid free BSA for 6 hr. Then the cells were washed with PBS and fixed with 4% paraformaldehyde. After the removal of formalin, cells were washed with PBS and stained with 0.2 % Oil Red O solution (Sigma-Aldrich) for 30 min, as described previously (McLaren et al., 2010). Cells were examined by light microscopy (× 400).

3-2-10 The expression of scavenger receptors

The expression of scavenger receptors, CD36 and SR-A, was measured by flow cytometry and western blot analysis. THP-1 cells (3×10^5 cells) were seeded on 24-well plates, exposed to suspended nanoparticles for 3 hr, and then differentiated to THP-1 monocytes/macrophages with 162 nM PMA. THP-1 monocytes/macrophages were evaluated for membrane CD36 or SR-A expression by the use of a primary anti-CD36 (Abcam) or a mouse IgG1 κ isotype control (BioLegend, San Diego, CA), and SR-A (R&D systems, Minneapolis, MN) or a mouse IgG2b κ isotype control (BioLegend). Then, the cells were stained with Alexa647 labeled anti-mouse IgG antibody (Life Technologies) and analyzed on a FACS Canto II flow cytometer with at least 10,000 events acquired for each sample.

For western blot analysis, THP-1 cells (8×10^5 cells) were seeded on 100 mm dishes, exposed to suspended nanoparticles for 3 hr, and then differentiated to THP-1 monocytes/macrophages as described above. Cells were lysed in RIPA lysis buffer and protein samples (n = 4 in each group) were separated by 4/20 % SDS-PAGE and transferred onto PVDF membranes. The membranes were incubated with rabbit-polyclonal antibodies to CD36 (Santa Cruz) at a dilution of 1:400 and to SR-A (Santa Cruz) at a dilution of 1:400. Protein expression levels were normalized relative to the level of β-actin protein in the same sample.

3-2-11Statistical analysis

All parameters were expressed as mean ± standard deviation (SD). Statistical analyses were performed using one-way analysis of variance (ANOVA) followed by Dunnett's post hoc test. A p value less than 0.05 was considered statistically significant.

3-3 Results

3-3-1 Characterization of suspensions of nanoparticles and cell viability

Both nanosized TiO_2 and ZnO were dispersed in the respective culture medium of HUVECs and THP-1. The intensity-weighted hydrodynamic average diameter of dispersed nanoparticles was measured by DLS technology. Table 1 shows the mean hydrodynamic diameters and PdI of dispersed TiO_2 or ZnO particles in each medium.

Although DLS data provided the mean hydrodynamic diameters of > 150 nm, the presence of nano-sized particles was confirmed in the medium (Table 1).

Table 1 Characterization of nanoparticles

Nanoparticles	Primary diameter (nm)	Manufacturer	Medium	Hydrodynamic size (nm)	PdI
TiO_2 (P25)	21	Degussa	RPMI1640 (10 % FBS)	189.6±1.08	0.140±0.006
			EBM-2 (2 % FBS)	160.4±0.75	0.265±0.009
ZnO	20	mkNANO	RPMI1640 (10 % FBS)	192.0±0.79	0.128±0.016
			EBM-2 (2 % FBS)	158.2±1.02	0.171±0.007

Data are mean ± SD of four independent experiments.

PdI: polydispersity index, RPMI: Roswell Park Memorial Institute, FBS: fetal bovine serum, EBM: endothelial basal medium

HUVECs were exposed to TiO_2 and ZnO particles at a concentration ranging from 1 to 100 μg/ml for 24 hr. The MTS assay showed that incubation of HUVECs in the presence of ZnO particles at 25 to 100 μg/ml, but not TiO_2 particles, significantly

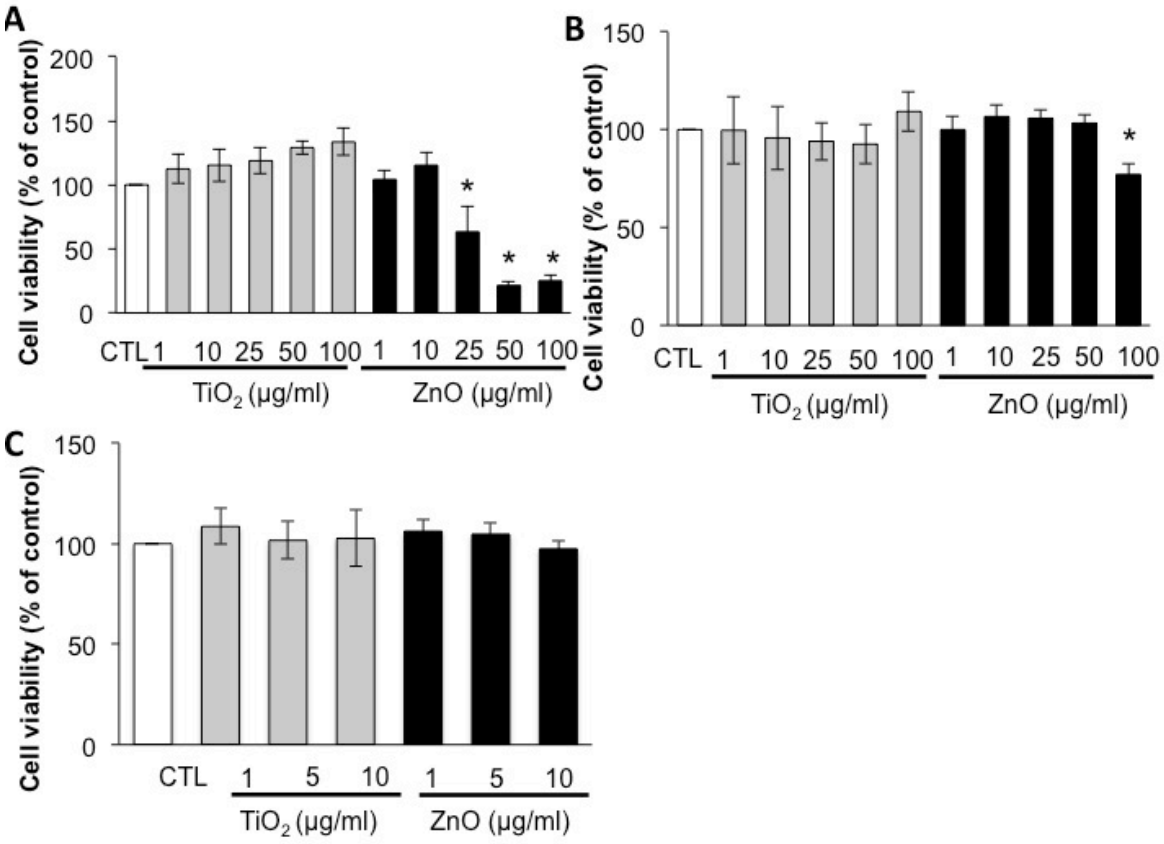

Fig. 1. Effects of TiO_2 and ZnO particles on cell viability. Cell viability was measured by MTS assay. (A) HUVECs were exposed to nanoparticles at a concentration ranging from 1 to 100 μg/ml for 24 h. (B) THP-1 monocytes were exposed to nanoparticles at a concentration ranging from 1 to 100 μg/ml for 3 h, and then treated with 162 nM PMA for 16 h in RPMI 1640 medium containing 10% FBS. (C) HUVECs were exposed to nanoparticles at a concentration ranging from 1 to 10 μg/ml for 16 hours. Data are mean ± SD of four experiments. *$p < 0.05$ vs. control (CTL).

reduced cell viability (Fig. 1A). In THP-1 monocytes/macrophages, cell viability was significantly decreased after exposure to 100 μg/ml of ZnO particles (Fig. 1B). The MTS assay showed that there were no significant changes in cell viability after incubation of HUVECs in the presence of ZnO particles at 1, 5, or 10 μg/ml for 16 hr (Fig. 1C). Therefore, we used nanoparticle concentrations below 10 μg/ml in the following experiments.

3-3-2 Amount of metal uptake and intracellular free zinc ion

The results of ICP-MS indicated that the amount of metal uptake in HUVECs correlated with the concentration of ZnO particles in the medium (Fig. 2A). The results also demonstrated a clear dose-dependent uptake of ZnO particles by HUVECs. On the other hand, only a small uptake of TiO_2 particles was noted in HUVECs (Fig. 2A). Moreover, we loaded HUVECs with a zinc-specific fluorescent (Zinquin ethyl ester) to visualize free intracellular zinc. Under control conditions, free intracellular zinc was not detected (Fig. 2B; panel a). After incubation of 10 μg/ml of ZnO particles for 16 hr, free intracellular zinc was observed (Fig. 2B; panel c) whereas no such signal was detected after exposure to 10 μg/ml of TiO_2 particles (Fig. 2B; panel b).

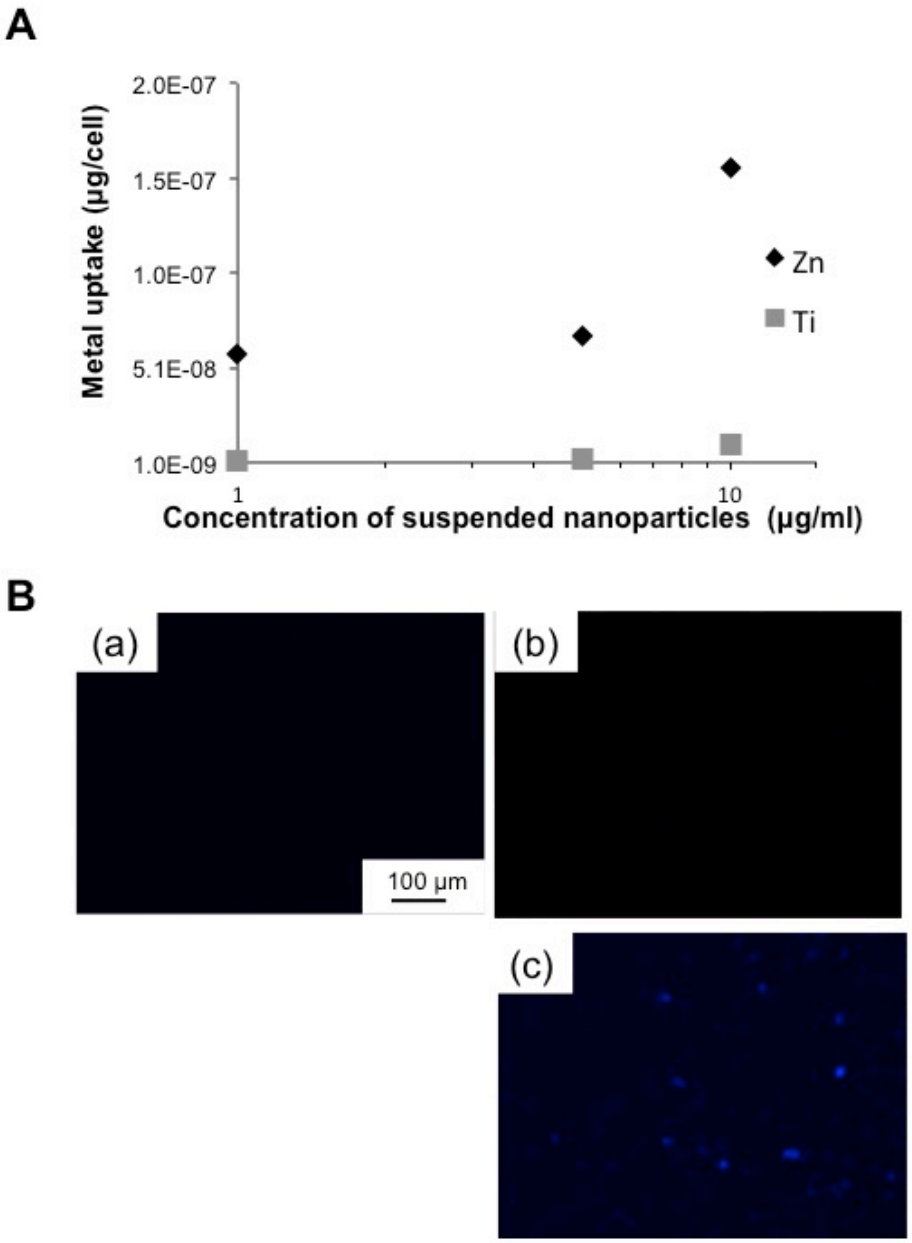

Fig. 2. Metal uptake and intracellular free zinc ion in HUVECs. (A) ICP-MS measurements of metal uptake by HUVECs. Relationship between the concentration of suspended nanoparticles in the medium (abscissa) and metal uptake (ordinate). (B) Visualization of intracellular free zinc ion in HUVECs exposed to 10 µg/ml of nanoparticles for 16 h. Panel (a) represents free zinc under control conditions. Panels (b) and (c) represent free zinc after exposure to TiO_2 and ZnO particles, respectively.

3-3-3 Effects of ZnO particles on monocyte migration and MCP-1 production

Given that monocyte migration is an important step that induces the adhesion of monocytes to endothelial cells, we measured the concentration of MCP-1 in supernatants of HUVECs after exposure to TiO_2 or ZnO nanoparticles. In a preliminary study, we measured MCP-1 levels after exposure of HUVECs to 10 μg/ml of ZnO particles for different times (4, 8, 16, or 21 hr) at 37 °C. We observed the significant increase in the concentration of MCP-1 after a 16-hour exposure (Fig. 3B). MCP-1 levels were then measured after exposure of HUVECs to different doses (1, 5, or 10 μg/ml) of TiO_2 or ZnO particles for 16 hr at 37 °C. Exposure to 10 μg/ml of ZnO particles significantly increased the concentration of MCP-1 (Fig. 3C), whereas exposure to TiO_2 particles had no effect on MCP-1 levels in the supernatants of HUVECs. Based on the marked increase in MCP-1 production in supernatants of HUVECs exposed to ZnO particles, we tested the effects of such supernatant on monocyte migration (Fig. 3A). The supernatant of HUVECs exposed to 10 μg/ml of ZnO particles significantly increased the number of THP-1 monocytes that passed through the Transwell microporous membrane, compared with the control (Fig. 3D). THP-1 monocyte migration was not observed in experiments using the supernatants of HUVECs exposed to TiO_2 particles.

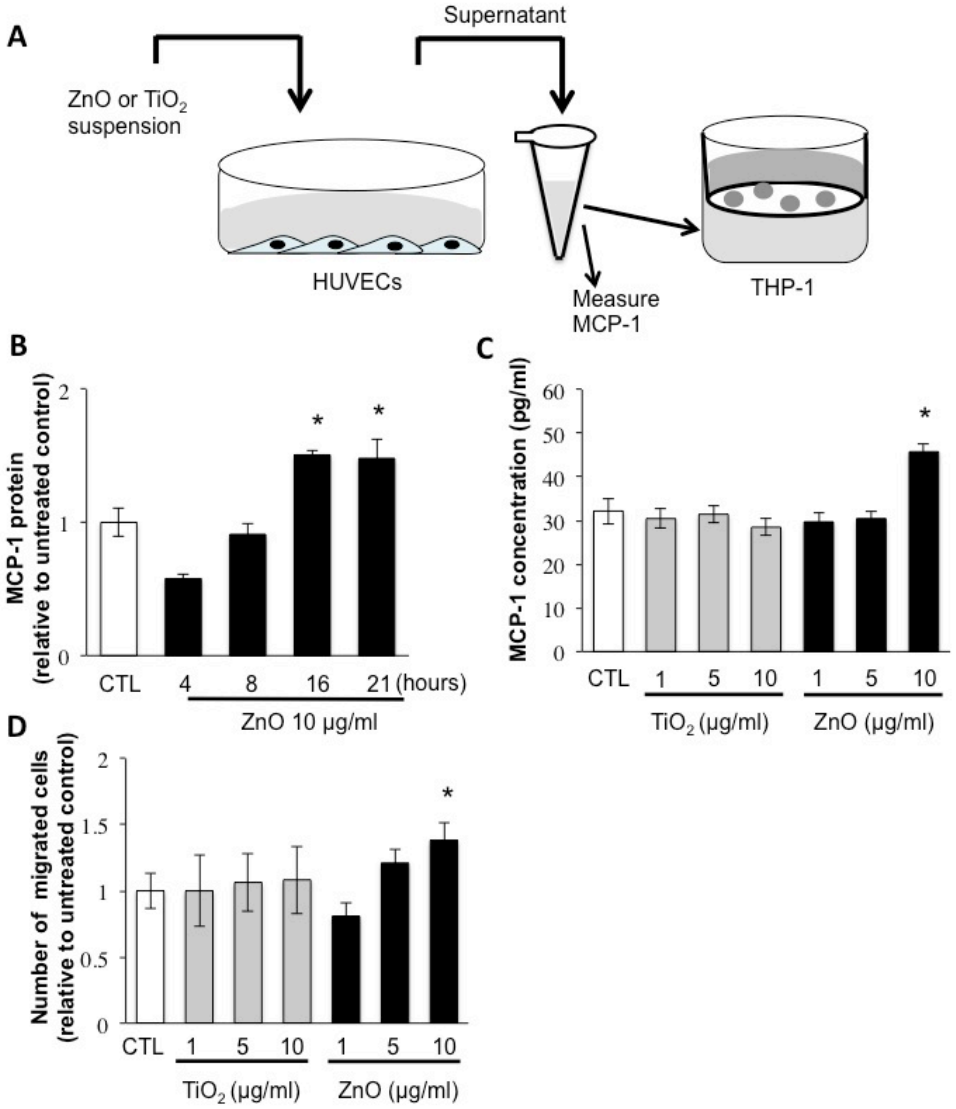

Fig. 3. MCP-1 production and THP-1 monocyte migration in supernatants of TiO_2 or ZnO nanoparticles-exposed HUVECs. (A) Schematic diagram representing the experimental procedure using the conditioned media. HUVECs were exposed to TiO_2 or ZnO particles for 16 h. The cells were centrifuged to remove any suspended nanoparticles. The supernatant was obtained and used for measurement of MCP-1 production as the chemoattractant. (B) The time-course of MCP-1 production after exposure to ZnO particles. MCP-1 levels were measured in HUVECs exposed to 10 μg/ml of ZnO particles for 4, 8, 16 or 21 hours. (C) MCP-1 production and (D) the relative number of migrated THP-1 monocytes after exposure to 1, 5, and 10 μg/ml of TiO_2 or ZnO particles. Data are mean ± SD of three experiments. *$p < 0.05$ vs. control (CTL).

3-3-4 Effects of ZnO particles on monocyte adhesion

To assess whether adhesion of THP-1 monocytes to HUVECs is enhanced by exposure to nanoparticles, we conducted adhesion assay of THP-1 monocytes to HUVECs after incubation with nanoparticles for 16 hr. Although the adhesion of THP-1 monocytes to HUVECs was not enhanced by TiO_2 particles (Fig. 4A; panels a, b), the number of adhering THP-1 monocytes was significantly increased by exposure to 5 and 10 μg/ml of ZnO particles (Figs. 4A, B; panel c).

Based on the above results, we then examined the expression of adhesion molecules in HUVECs (Fig. 5A). The expression level of ICAM-1 was significantly higher in HUVECs exposed to 10 μg/ml of ZnO particles than the control (Fig. 5B). On the other hand, exposure of HUVECs to both TiO_2 and ZnO particles did not change the expression of VCAM-1 (Fig. 5C).

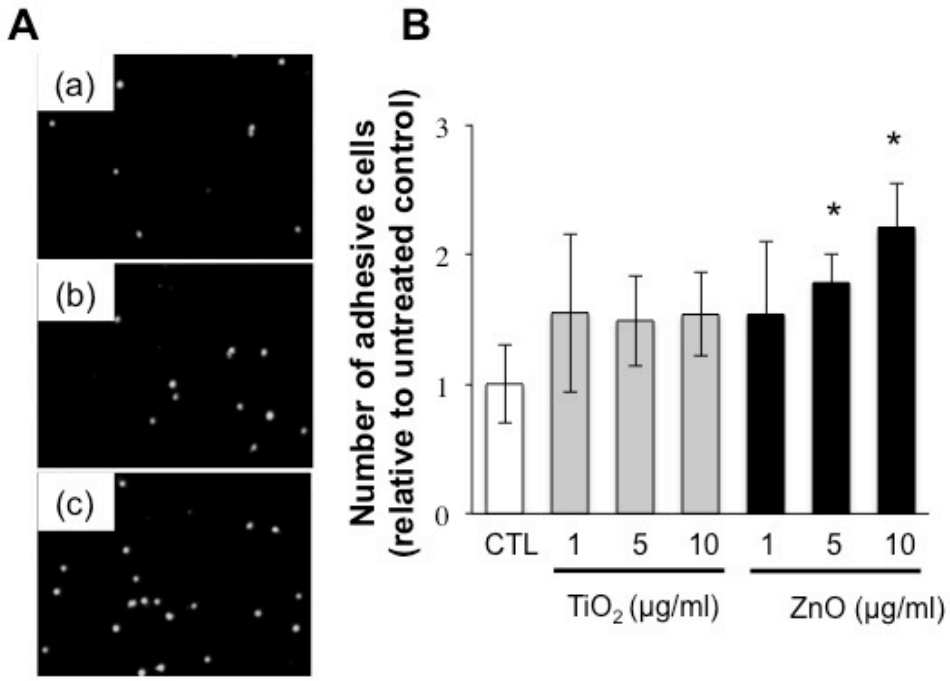

Fig. 4. Adhesion assay of THP-1 monocytes to HUVECs. (A) Representative images of THP-1 monocyte adhesion to HUVECs. Panel (a) represents image under control conditions. Panels (b) and (c) represent the adhesion of THP-1 cells to HUVECs after exposure to 10 μg/ml of TiO_2 and ZnO particles, respectively. (B) Relative number of adhesive THP-1 monocytes to HUVECs after exposure to TiO_2 or ZnO particles (1–10 μg/ml) for 16 h. Data are mean ± SD of four experiments. *$p < 0.05$ vs. control (CTL).

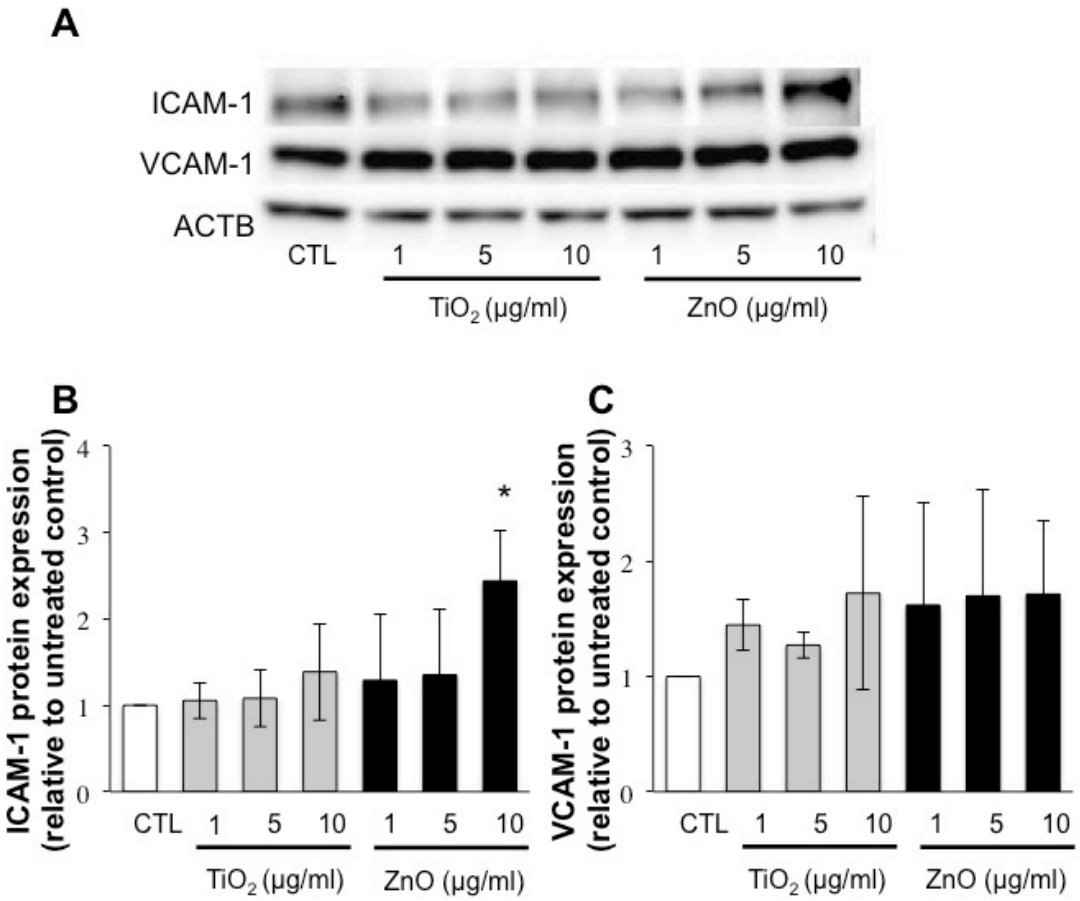

Fig. 5. Expression of adhesion molecule proteins in HUVECs.
(A) Representative images of western blot analysis of ICAM-1 and VCAM-1 in HUVECs exposed to 1–10 μg/ml of TiO_2 or ZnO particles. Relative quantitative expression levels of (B) ICAM-1 and (C) VCAM-1 in HUVECs exposed to TiO_2 or ZnO particles. Data are mean ± SD of three or four experiments. *$p < 0.05$ vs. control (CTL).

3-3-5 Effects of ZnO particles on Ac-LDL uptake in THP-1 monocytes/macrophages

To investigate the roles of TiO_2 and ZnO particles on foam cell formation, we first measured the uptake of Ac-LDL, which is a type of LDL extensively used in in vitro foam cell formation assays. THP-1 monocytes were exposed to 1, 5, 10 μg/ml of TiO_2 and ZnO particles for 3 hr, and then THP-1 monocytes were differentiated into macrophage using PMA. DiI-AcLDL uptake was significantly increased following exposure to 5 and 10 μg/ml of ZnO particles in THP-1 monocytes/macrophages (Figs. 6A, B).

In contrast, DiI-AcLDL uptake did not change in cells exposed to TiO_2 particles. Consistent with the above results on Ac-LDL uptake by flow cytometer, Oil Red staining showed that exposure to 10 μg/ml of ZnO particles significantly promoted lipid accumulation in THP-1 monocytes/macrophages after Ac-LDL uptake (Fig. 7).

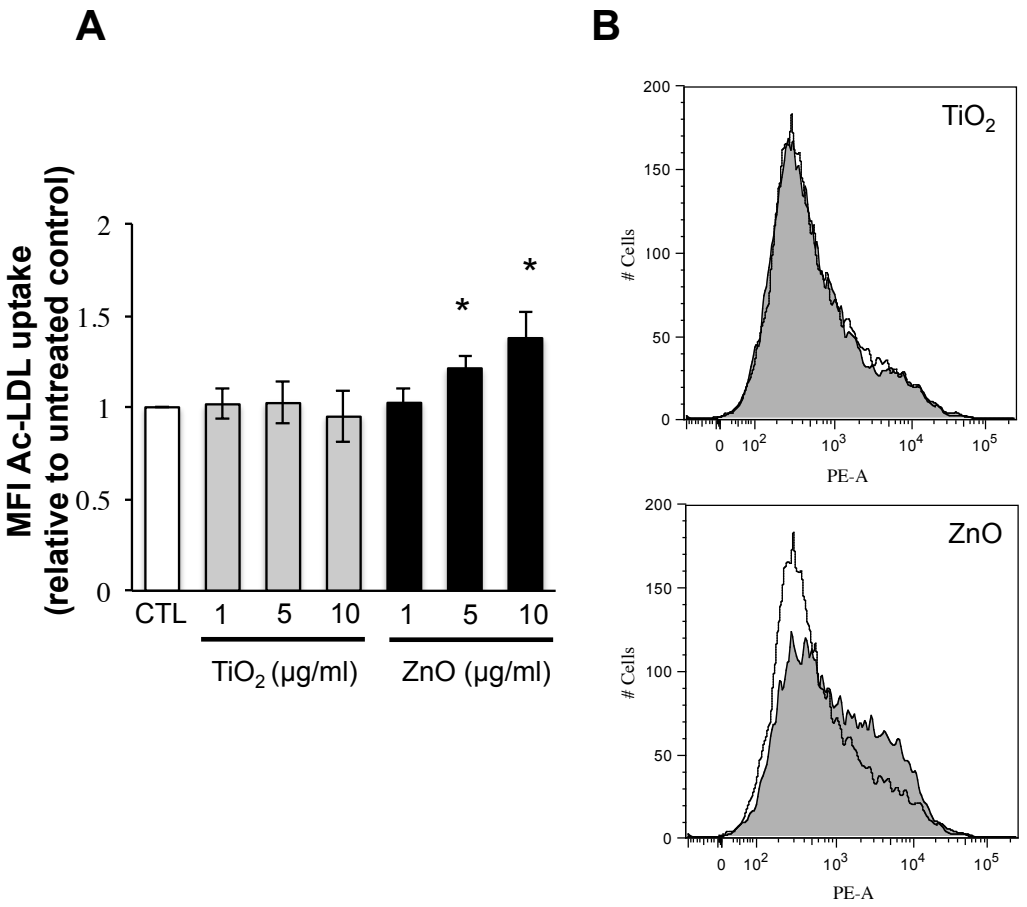

Fig. 6. Assessment of TiO_2 or ZnO particle-exposure on Ac-LDL uptake by PMA-stimulated THP-1 monocytes/macrophages. (A) Quantitative data of DiI-AcLDL uptake by THP-1 monocytes/macrophages differentiated after exposure to TiO_2 or ZnO particles (1–10 µg/ml) for 3 h. The differentiated THP-1 cells were incubated at 37 °C with 10 µg/ml of DiI-AcLDL for 6 h. (B) Representative FACS images of DiI-AcLDL uptake by THP-1 monocytes/macrophages. Data are mean ± SD of six experiments. *$p < 0.05$ vs. control (CTL).

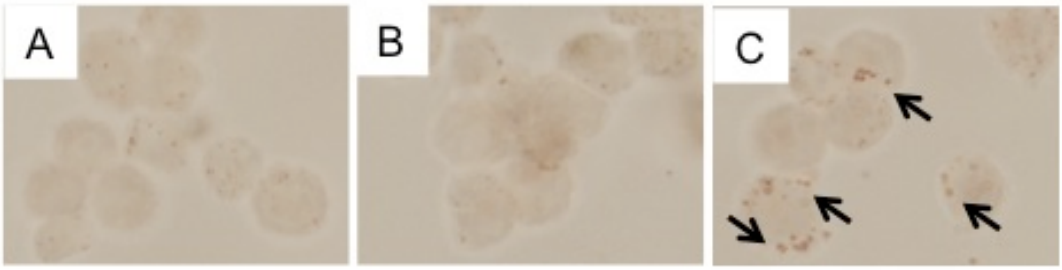

Fig. 7. Oil Red O staining of THP-1 monocytes/macrophages. (A) Cells were fixed and stained with Oil Red O solution under control conditions. Panels (B) and (C) represent Oil Red O staining of THP-1 monocytes/macrophages incubated at 37 °C with 10 μg/ml of Ac-LDL for 6 h. THP-1 monocytes differentiated after exposure to 10 μg/ml of TiO_2 or ZnO particles, respectively. Arrows show intracellular lipid accumulation stained with Oil Red O solution.

3-3-6 Effects of ZnO particles on CD36 and SR-A expression in THP-1 monocytes/macrophages

Finally, we tested the effects of TiO_2 and ZnO particles on the expression of scavenger receptors, such as CD36, and SR-A. These receptors are known to bind and internalize both Ac-LDL and oxidized-LDL. For this purpose, we exposed THP-1 monocytes to 1, 5, 10 μg/ml of TiO_2 and ZnO particles for 3 hr, and then differentiated the THP-1 monocytes into macrophage with PMA. Exposure to ZnO particles increased the expression levels of SR-A in THP-1 monocytes/macrophages in a dose-dependent manner (Figs. 8A, B). Significant increases in CD36 expression were also noted after exposure to 10 μg/ml of ZnO particles as demonstrated by flow cytometry (Figs. 8C, D). On the other hand, exposure to TiO_2 particles decreased CD36 expression but did not change SR-A expression (Figs. 8A, C).

We also examined the expression levels of CD36 and SR-A in THP-1 monocytes/macrophages by western blot analysis. The results showed that exposure to 10 μg/ml of ZnO particles increased CD36 and SR-A expression in THP-1 monocytes/macrophages compared with the control (Figs. 9A–C).

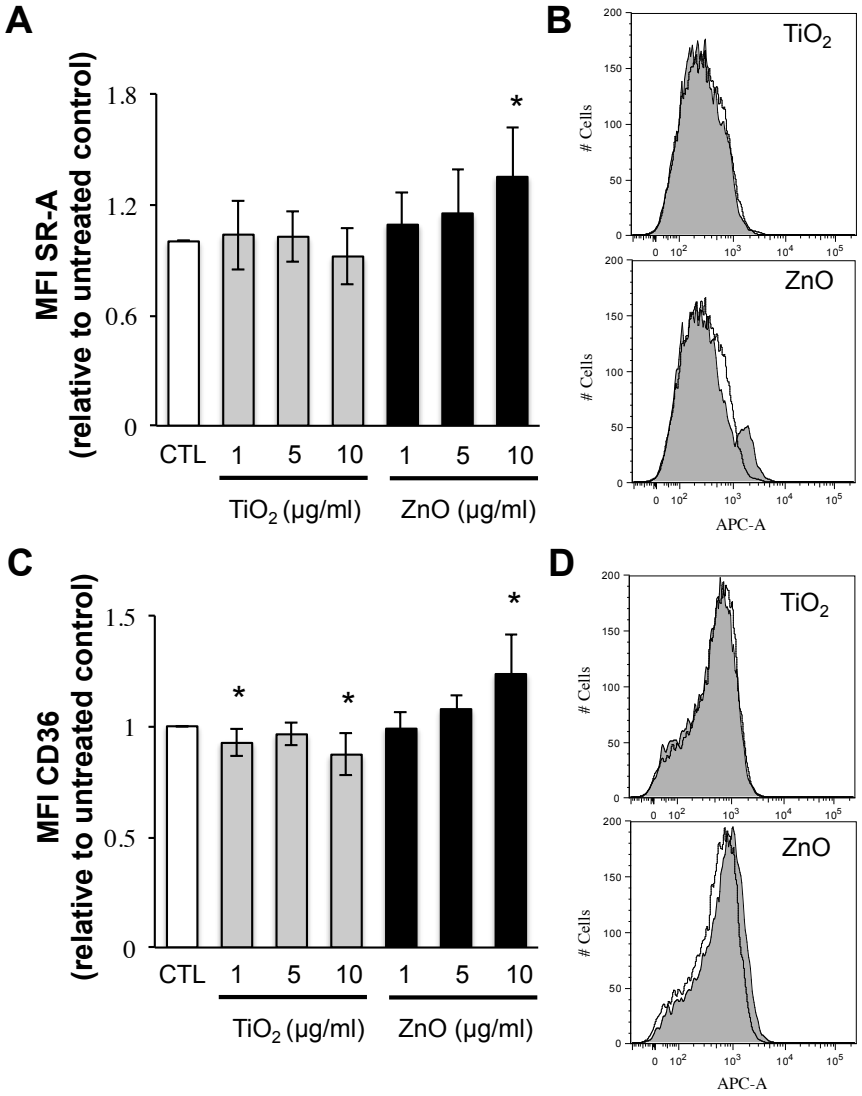

Fig. 8. Effects of exposure to TiO_2 or ZnO particles on the expression of scavenger receptors. Quantitative data of (A) SR-A (n = 9) and (C) CD36 (n = 7) in THP-1 monocytes/macrophages differentiated after exposure to TiO_2 or ZnO particles (1–10 µg/ml) for 3 h. Representative FACS assessment of (B) SR-A and (D) CD36 protein. Data are mean ± SD. *$p < 0.05$ vs. control (CTL).

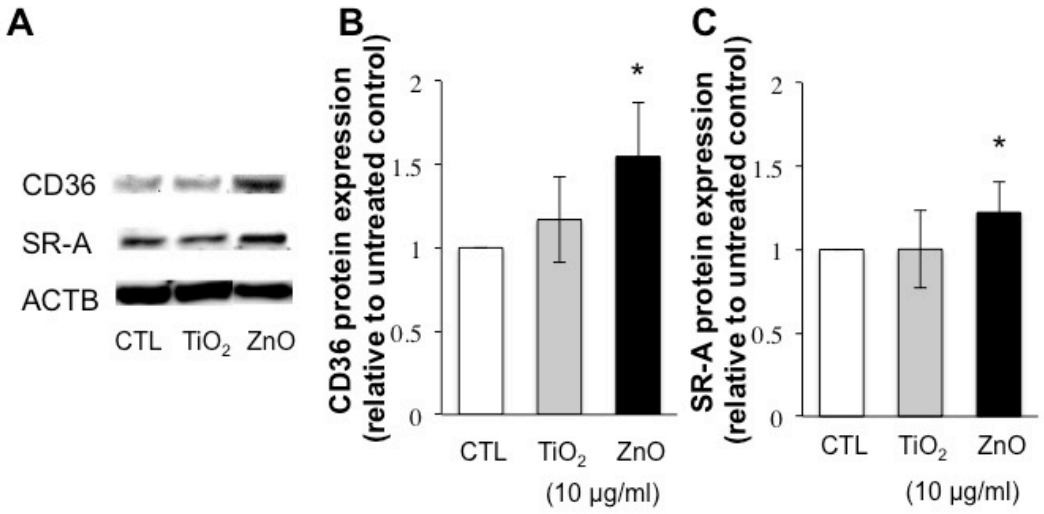

Fig. 9. Quantification of SR-A and CD36 expression levels. (A) Representative images of western blot analysis in THP-1 monocytes/macrophages differentiated after exposure to TiO_2 or ZnO particles (10 μg/ml) for 3 h. Expression levels of (B) SR-A and (C) CD36 in THP-1 monocytes/macrophages (n = 4 or 6). Data are mean ± SD. *$p < 0.05$ vs. control (CTL).

3-4 Summary

The present study demonstrated that exposure to ZnO nanoparticles induced cell migration mediated by increased MCP-1 level and adhesion of THP-1 cells to HUVECs. We also demonstrated that exposure to the same nanoparticles increased cholesterol uptake in THP-1 monocytes/macrophages due to the upregulation of membrane scavenger receptors of modified LDL, leading to foam cell formation.

3-6 References

B.C. Berk. Atheroprotective signaling mechanisms activated by steady laminar flow in endothelial cells. Circulation, (2008) 117, pp. 1082–1089.

I.F. Charo, M.B. Taubman. Chemokines in the pathogenesis of vascular disease. Circ. Res., (2004) 95, pp. 858–866.

A. Gojova, B. Guo, R.S. Kota, J.C. Rutledge, I.M. Kennedy, A.I. Barakat. Induction of inflammation in vascular endothelial cells by metal oxide nanoparticles: effect of particle composition. Environ. Health Perspect., (2007) 115, pp. 403–409.

P. Libby, P.M. Ridker, G.K. Hansson. Leducq transatlantic network on atherothrombosis: inflammation in atherosclerosis: from pathophysiology to practice. J. Am. Coll. Cardiol., (2009) 54, pp. 2129–2138.

A.J. Lusis. Atherosclerosis. Nature, (2000) 407, pp. 233–241.

K.J. Moore, M.W. Freeman. Scavenger receptors in atherosclerosis: beyond lipid uptake. Arterioscler. Thromb. Vasc. Biol., (2006) 26, pp. 1702–1711.

R.C. Murdock, L. Braydich-Stolle, A.M. Schrand, J.J. Schlager, S.M. Hussain. Characterization of nanomaterial dispersion in solution prior to in vitro exposure using dynamic light scattering technique. Toxicol. Sci., (2008) 101, pp. 239–253.

G. Oberdörster, E. Oberdörster, J. Oberdörster. Nanotoxicology: an emerging discipline evolving from studies of ultrafine particles. Environ. Health Perspect., (2005) 113, pp. 823–839.

J. Oh, A.E. Riek, S. Weng, M. Petty, D. Kim, M. Colonna, M. Cella, C. Bernal-Mizrachi. Endoplasmic reticulum stress controls M2 macrophage differentiation and foam cell formation. J. Biol. Chem., (2012) 287, pp. 11629–11641.

C.A. Shaw, S. Robertson, M.R. Miller, R. Duffin, C.M. Tabor, K. Donaldson, D.E. Newby, P.W. Hadoke. Diesel exhaust particulate–exposed macrophages cause marked endothelial cell activation. Am. J. Respir. Cell Biol., (2011) 44, pp. 840–851.

S. Tsimikas, Y.I. Miller. Oxidative modification of lipoproteins: mechanisms, role in inflammation and potential clinical applications in cardiovascular disease. Curr. Pharm. Des., (2001) 17, pp. 27–37.

W. Wu, G. Ichihara, Y. Suzuki, K. Izuoka, S. Oikawa-Tada, J. Chang, K. Sakai, K. Miyazawa, D. Porter, V. Castranova, M. Kawaguchi, S. Ichihara. Dispersion method for safety research on manufactured nanomaterials. Ind. Health, (2013) 52, pp. 54–65.

4. Discussion

4-1 Which sonicator type is suitable to disperse nanomaterials?

Prior to the evaluation of dispersion condition, adjustment of appropriate particle concentration for DLS measurement was performed following the recommendations of the instrument instructions. According to the instructions, particle concentration is a factor for the accuracy of measurement, and sufficient opaqueness is suggested to accommodate the optical requirements of DLS. TiO_2 nanoparticles showed the smallest hydrodynamic diameter and deviation at the concentration of 25 μg/ml. At higher or lower concentrations than 25 μg/m, variability of hydrodynamic diameter became greater, probably due to instable translational diffusion coefficient of Brownian motion resulting from changes in particle interaction. Although further study is needed to ensure whether the measured diameter was concentration dependent or not, the concentration of 25 μg/ml was optimal for size characterization of TiO_2 nanoparticles with regard to the least deviation. By contrast, smaller peak 1 and especially lower PdI were observed in samples of higher concentration of ZnO nanoparticles. The higher PdI value derived from lower concentrations can be explained by the bimodal size distribution. Because of the similar refractive index between ZnO nanoparticles and DM, the light scattering intensity of DM turned out to be a certain proportion of the total recorded intensity and the quality of resulting DLS data was too poor to be interpreted correctly. In this situation, the light scattering intensity of nanoparticles could be enhanced by using elevated particle concentration, and good quality of DLS data was obtained at the concentration of 500 μg/ml in the

present study. In case of size distribution with more than one peak, z-average, which is calculated from total detected intensity, is not suitable for description of particle size distribution. It is therefore advisable to use peak 1, the peak value of the principal peak of the intensity-weighted hydrodynamic diameter distribution, to compare the outcomes of DLS. It is worth noting that determination of proper concentration should be conducted for each nanomaterial and the selected concentration should be reported.

Direct probe-type sonicator is usually recommended over indirect bath/cup-type sonicator based on the higher efficacy in energy delivery into the suspension, without energy loss generated from the process that ultrasonic waves pass through both the bath/cup liquid and the wall of the sample container, and thus is widely used in safety research on nanomaterials (Hussain et al., 2010, Lu et al., 2009, Sager et al., 2009 and Shvedova et al., 2005). However, large variance is often encountered due to technical problems such as uncertainty in probe immersion position. Moreover, direct immersion of the probe into the suspension could introduce contamination of the sample at the same time. Although such contamination could be avoided, an unavoidable side effect of the probe-type is tip erosion, which was observed in our study. In addition, tip erosion also induces reduction of energy (Taurozzi et al., 2011), resulting in subsequent alteration of dispersion condition that is critical to data reproducibility. Furthermore, samples are usually left on the bench in uncovered containers. Thus, the evaporative loss of liquid content and deposition of dust should be taken into consideration as well.

On account of the aforementioned problems with probe-type sonicator, the cup-type sonicator was utilized for further analysis. Effective energy delivery was achieved by

minimal interspace between the sample container and the internal layer of the cup, which contributed to significant minimization of energy loss. Simultaneously, due to the massive collapse of the bubbles and the high local energy generated, excessive heating cycles occur at the interface of the explosion. A rapid rise in liquid temperature is an inherent effect in both direct and indirect sonication (Taurozzi et al., 2011). In order to avoid overheating of the suspension along with consequent liquid evaporation or degradation of the medium components, a circulatory cooling system was used in this study. Smaller agglomerates and better monodispersion of TiO_2 nanoparticles was produced within shorter dispersion time by sonication at cooling water temperature of 5°C rather than −10°C. It is speculated that if the cooling water is set at an extremely low temperature, the cup-type sonicator may be frozen by the circulation, and this may induce inefficiency of sonication, resulting in subsequent poor dispersion of TiO_2 nanoparticle suspension. Moreover, effect of medium temperature on the particle interaction and size distribution needs to be studied further.

Besides the impact of temperature of cooling water, dispersion time and output power of sonicator play important roles in nanomaterials dispersion as well. Decrease in the secondary dynamic diameters of TiO_2 and ZnO nanoparticles resulted from increased dispersion time or output power using probe-type or cup-type sonicator, respectively. This suggested that more delivered energy which was derived from increased dispersion time or output power of sonicator contributed to break the bonds within agglomerates and disrupt the formation of agglomeration. The asymptotic behavior of the size change with output power of sonicator observed in the present study is consistent with the findings of previous studies (Bihari et al., 2008 and

Hielsher., 2005). The secondary diameters ceased to change after a critical output power value, indicating that nanomaterials in suspensions cannot be dispersed to their primary sizes and that the presence of at least a minimal number of agglomerates should always be expected in safety research (Taurozzi et al., 2011 and Poter et al., 2008).

In actual nanosafety research, samples with different concentrations of nanomaterials are required for dose-response experiments. Thus, we tested the effect of particle concentration on size distribution. TiO_2 and ZnO nanoparticles were sonicated at concentration of 0.5 or 2.5 mg/ml, and the size characterization was conducted. As a result, particle concentration at 0.5 or 2.5 mg/ml did not show an obvious effect on size distribution of TiO_2 nanoparticles, while reduction of the secondary diameter of ZnO nanoparticles was observed at higher concentration. In principle, higher particle concentration leads to increased particle collision frequency which can enhance particle breakage but also induce agglomerate formation at the same time. The discrepancy between TiO_2 and ZnO nanoparticles is due to the different physiochemical properties of each material, including different breakage behavior and/or surface interaction with components of the medium (Murdock et al., 2008 and Taurozzi et al., 2011). Such issues need to be investigated in future studies. The results highlight the demand to characterize the size distribution when dispersion of specific particles is operated at different concentrations. It is also important to report the dispersion concentration to allow comparisons between studies from different laboratories.

Stable dispersion status is usually desirable for studies spanning over days. Therefore,

the stability of TiO_2 and ZnO nanoparticles suspension was assessed until the 7th days after sonication. Agglomerates of TiO_2 and ZnO nanoparticles increased slightly by only 10 % and 5 %, respectively, which was acceptable for safety evaluation of nanomaterials. Furthermore, alteration of output power from 100 to 220 W did not change the size distribution of TiO_2 and ZnO nanoparticles soon after sonication and both prevented the reagglomeration of nanoparticles for at least 7 d after dispersion. Since the sample was extremely heated when sonicated for more than 10 min, dispersion time was limited to 10 min. Thus sonication can be operated with the maximum output power of 220 W for more energy delivery, but the results of stability demonstrated that desired degree of particle dispersion can be achieved with less output power of 100 W. In order to avoid overloading the sonicator and to minimize unwanted side effects (Taurozzi et al., 2011), we established the best dispersion protocol as followed: cup-type sonicator, with output power of 100 W, 80% pulse mode, for 10 min.

The protocol was set up based on TiO_2 and ZnO nanoparticles and further application to dispersion of MWCNTs was checked. Size characterization of nanotubes by DLS is not accurate (Taurozzi et al., 2011), and thus optical microscopy and TEM were used for morphological observation. MWCNTs clusters were not able to be disrupted after one single sonication following this protocol. After cooling, another 10-min sonication was performed and MWCNTs were dispersed into smaller bundles consequently. As previously demonstrated in the section that described the effect of dispersion time, higher energy was delivered into the suspension by prolonged dispersion time to break the bonds within the agglomerates of nanoparticles, indicating that this procedure can

also be applied to nanotubes. With regard to the side effect of temperature, the dispersion time should be extended by repeating the 10 min sonication rather than selecting continuous operation in the present cup-type sonicator protocol.

It is worth mentioning that this protocol is not for all dispersion systems for different nanomaterials, media, sonicators, and sample containers. We here outlined the procedure and key points for a dispersion optimization study that is essential to start nanotoxicological research. Application of this protocol to other dispersion systems is feasible by adjustment of dispersion time, output power of sonicator or particle concentration.

4-2 How do ZnO nanoparticles induce atherosclerosis *in vitro*?

What is the mechanism of the effects of ZnO nanoparticles on these atherosclerogenesis processes? Previous studies suggested that accumulation of inhaled particles in the lungs may cause systemic inflammation through oxidative stress, which mediates endothelial dysfunction and atherosclerosis (Araujo et al., 2008). In addition, these particles are also thought to increase blood coagulability through the activation of platelets and enhancement of autonomic nervous system via pulmonary reflexes, leading to increased risk of cardiovascular diseases (Seaton et al., 1995). Recent studies demonstrated that nanosized particles can cross the pulmonary epithelial barrier and enter the bloodstream (Liao et al., 1999 and Nemmar et al., 2002), and that these particles are barely recognized by phagocytosing cells, such as macrophages (Kreyling et al., 2002). These results suggest that nanoparticles could be taken up by endothelial cells and potentially interact directly with endothelial cells to

induce injury and inflammation. Therefore, we focused in the present study on the direct effects of metal oxide nanoparticles on cultured vascular endothelial cells in order to explore the cellular mechanisms responsible for the cardiovascular effects of nanoparticles.

Given that particle agglomeration and inadequate dispersion preferentially influence their toxicity, dispersion should be optimized under physiological conditions (Sager et al., 2007). In a preliminary study, we used various output power levels of the cup-type sonicator to optimize the dispersion of nanoparticles. Although the size of the agglomerated nanoparticles measured by the DLS technology appeared to decrease with increased output power, the maximum reduction reached a plateau level at output power of 100 W. PdI also showed the same trend. Therefore, in the present study, we dispersed suspensions of nanoparticles at concentration of 1.0 mg/ml by the cup-type sonicator at 100 W, 80 % pulsed mode, for 15 min (Wu et al., 2013). We observed the dispersed nanoparticles by transmission electron microscope (TEM) and confirmed that the samples were well dispersed by sonication at 100 W.

The association between endothelial cell injury/inflammation and the development of atherosclerosis is well known (Ross, 1999). Injury of endothelial cells promotes the migration of mononuclear cells and triggers the attachment of leukocytes to the subendothelial region, initiating atherosclerosis. MCP-1 plays an important role in the early recruitment of monocytes to atherosclerosis lesions (Charo and Taubman, 2004). In the present study, exposure of HUVEC to ZnO particles significantly increased the concentration of MCP-1. These results are consistent with a previous study that showed an increased level of MCP-1 in human aortic endothelial cells (HAECs) in a

dose-dependent manner after exposure to ZnO nanoparticles (Gojova et al., 2007). In addition, we newly showed a significant increase in the number of THP-1 monocytes that migrated through membrane micropores following the addition of supernatant of HUVECs exposed to ZnO particles. Our results indicate that exposure of endothelial cells to ZnO particle increases in the concentration of MCP-1 and induces monocyte migration.

The present study also showed that exposure of HUVECs to ZnO particles significantly up-regulated the expression level of ICAM-1. These results are consistent with previous studies that showed ZnO particle-induced increase in ICAM-1 expression in endothelial cells (Li et al., 2012 and Tsou et al., 2010). ZnO nanoparticles seem to provoke endothelial ICAM-1 expression through the Ras-related C3 botulinum toxin substrate 1 (Rac1)/cell division control protein 42 homolog (Cdc42)-mixed lineage kinase 3 (MLK3)-c-Jun N terminal kinase (JNK) pathway (Li et al., 2012). ICAM-1 binds and interacts with leukocyte integrin receptors and provides an adaptive alternative in the adhesion process between circulating cells and the endothelium, leading to the attachment of leukocytes to endothelial cells and to the accumulation of leukocytes in the vascular wall (Van de Stolpe and van der Saag, 1996). In this way, ICAM-1 could mediate the assembly of monocytes, macrophages, T lymphocytes, and platelets and their adhesion to the vascular wall, which plays a key role in the pathogenesis of atherosclerosis (Ley et al., 2011). In the present study, we conducted adhesion assay of THP-1 monocytes to HUVECs and confirmed that adhesion of THP-1 monocytes to HUVECs was enhanced by exposure to ZnO particles.

The association between exposure to nanoparticle and cardiovascular diseases has recently raised concern about the safety of various nanoparticles. So far, the reported harmful effects include endothelial cell proliferation, altered vascular reactivity, and increased vascular inflammation both in vitro (Yamawaki and Iwai, 2006 and Zhu et al., 2011) and in vivo (Mikkelsen et al., 2011 and Xu et al., 2012). Studies using apolipoprotein E knockout (ApoE-KO) mice, an animal model of atherosclerosis, showed that instillation of single-walled carbon nanotubes (SWCNTs) was associated with slightly larger plaque area in the aorta compared with the controls in mice on high-fat diet (Li et al., 2007). In ApoE-KO mice exposed to ZnO nanoparticles, atherosclerotic plaques and foam cells identified by Oil Red O staining were mainly present in the intima and medial areas of the arterial wall (Li et al., 2012). Consistent with this study, Oil Red staining in the present study showed that the exposure to ZnO particles significantly promoted the uptake of Ac-LDL and increased intracellular lipid accumulation in THP-1 monocytes/macrophages. Furthermore, although Ac-LDL uptake was significantly increased by exposure to ZnO particles, the uptake did not change in cells exposed to TiO_2 particles. One previous study demonstrated a modest increase in plaque progression in the aorta of mice by the instillation of nanosized TiO_2 particles (Mikkelsen et al., 2011). Further investigation is needed to determine the effects of nanosized TiO_2 particles on the formation of foam cells.

Foam cells are the hallmark of atherosclerosis and their formation is crucial in the initiation and progression of atherosclerosis. As one of the critical steps in foam cell formation, macrophages take-up the oxidized LDL via scavenger receptors in a process that converts them into foam cells (Rader and Pure, 2005). The uptake of

Ac-LDL and oxidized LDL into macrophages involves a family of scavenger receptors, including SR-A and CD36, which are known to bind and internalize both forms of LDL (Pluddemann et al., 2007). Macrophage scavenger receptors play a decisive role in transforming macrophage into foam cells (Rader and Pure, 2005). In the present study, we observed significant increases in CD36 and SR-A expression in THP-1 monocyte/macrophage following exposure to ZnO particles. These results suggest that ZnO particles modulate the expression of CD36 and SR-A, which are involved in the uptake of modified LDL. The measurement by flow cytometry showed that exposure to TiO_2 particles significantly decreased CD36 expression in THP-1 monocytes/macrophages. However, there was no change in the expression of CD36 after exposure to 10 μg/ml of TiO_2 particles by western blot analysis. After exposure to TiO_2 particles, not ZnO particles, both forward scatter (corresponding to cell size) and side scatter (corresponding to cell granularity or internal complexity) signals were significantly changed (data not shown). These changes in THP-1 monocytes/macrophages exposed to TiO_2 particles might affect the value of the mean fluorescence intensity of CD36. Further studies will be needed to demonstrate that conclusively.

Metal oxide nanoparticles are newly developed materials used in a variety of applications. Nanosized ZnO and TiO_2 have been applied extensively in different fields, including industry, cosmetics, and biomedicines. It has been reported that ZnO particles induce inflammation and are cytotoxic in mammalian cells (Li et al., 2012 and Tsou et al., 2010). Previous studies suggested that dissolved zinc ions seem to be the culprit in the toxic effects of ZnO particles (Song et al., 2010) and demonstrated

that exposure to zinc ions [soluble zinc compounds; $Zn(NO_3)_2$ and $Zn(CH_3COO)_2$] alone was sufficient to induce inflammatory changes of severity similar to that observed with ZnO particles in vascular endothelial cells (Yeh et al., 2011). On the other hand, exposure of endothelial cells to ZnO particles was followed by their direct penetration of the cell membrane and their identification in the cytoplasm (Gojova et al., 2007 and Li et al., 2012). These studies suggest that ZnO particle-induced responses were to a large extent dependent on particle size rather than on the releases of zinc ions (Li et al., 2012 and Sharma et al., 2012). Another study demonstrated that a rapid, pH-dependent dissolution of ZnO nanoparticles inside the phagosomes is the main cause of ZnO nanoparticle-induced tissue injury (Cho et al., 2011). The present study demonstrated a significance correlation between the amount of metal uptake and the concentration of ZnO particles in the supernatants, as determined by ICP-MS, and an increase in free intracellular zinc ions in HUVECs exposed to ZnO particles. While it is uncertain whether zinc was mainly ionized after the entry of ZnO particles into the cells or whether the dissolved zinc ions entered the cells, our results suggest that the dissolved zinc ions in the cells can induce monocyte chemotactic factor and adhesion molecules as well as acceleration of migration and adhesion. Further studies are needed to clarify whether ZnO nanoparticle-induced responses are dependent on particle size or released zinc ions.

4-3 Refference

J.A. Araujo, B. Barajas, M. Kleinman, X. Wang, B.J. Bennett, K.W. Gong, M. Navab, J. Harkema, C. Sioutas, A.J. Lusis, A.E. Nel. Ambient particulate pollutants in the ultrafine range promote early atherosclerosis and systemic oxidative stress. Circ. Res., (2008) 102, pp. 589–596.

P. Bihari, M. Vippola, S. Schultes, M. Praetner, A.G. Khandoga, C.A. Reighel, C. Coester, T. Tuomi, M. Rehberg, F. Krombach. Optimized dispersion of nanopartciles for biological *in vitro* and *in vivo* studies. Part. Fibre Toxicol., (2008) 5, p. 14.

W.S. Cho, R. Duffin, S.E. Howie, C.J. Scotton, W.A. Wallace, W. Macnee, M. Bradley, I.L. Megson, K. Donaldson. Progressive severe lung injury by zinc oxide nanoparticles; the role of Zn^{2+} dissolution inside lysosomes. Part. Fibre Toxicol., (2011) 8, p. 27.

W. Choi, S.Y. Eum, Y.W. Lee, B. Hennig, L.W. Robertson, M. Toborek. PCB 104-induced proinflammatory reactions in human vascular endothelial cells: relationship to cancer metastasis and atherogenesis. Toxicol. Sci., (2003) 75, pp. 47–56.

A. Gojova, B. Guo, R.S. Kota, J.C. Rutledge, I.M. Kennedy, A.I. Barakat. Induction of inflammation in vascular endothelial cells by metal oxide nanoparticles: effect of particle composition. Environ. Health Perspect., (2007) 115, pp. 403–409.

Y. Hielsher. Ultrasonic production of nano-size dispersions and emulsions. Dans European Nano Systems Workshop − ENS 2005.

S. Hussain, L.C. Thomassen, I. Ferecatu, M.C. Borot, K. Andreau, J.A. Martens, J. Fleury, A. Baeza-Squiban, F. Marono, S. Boland. Carbon black and titanium dioxide nanoparticles elicit distinct apoptotic pathways in bronchial epithelial cells. Part. Fibre Toxicol., (2010) 7, p. 10.

W.G. Kreyling, M. Semmler, F. Erbe, P. Mayer, S. Takenaka, H. Schulz, G. Oberdörster, A. Ziesenis. Translocation of ultrafine insoluble iridium particles from lung epithelium to extrapulmonary organs is size dependent but very low. J. Toxicol. Environ. Health A., (2002) 65, pp. 1513–1530.

K. Ley, Y.I. Miller, C.C. Hedrick. Monocyte and macrophage dynamics during atherogenesis. Arterioscler. Thromb. Vasc. Biol., (2011) 31, pp. 1506–1516.

Z. Li, T. Hulderman, R. Salmen, R. Chapman, S.S. Leonard, S.H. Young, A. Shvedova, M.I. Luster, P.P. Simeonova. Cardiovascular effects of pulmonary exposure to single-wall carbon nanotubes. Environ. Health Perspect., (2007) 115, pp. 377–382.

C.H. Li, P.L. Liao, M.K. Shyu, C.W. Liu, C.C. Kao, S.H. Huang, Y.W. Cheng, J.J. Kang. Zinc oxide nanoparticles-induced intercellular adhesion molecule 1 expression requires Rac1/Cdc42, mixed lineage kinase 3, and c-Jun N-terminal kinase activation in endothelial cells. Toxicol. Sci., (2012) 126, pp. 162–172.

D. Liao, J. Creason, C. Shy, R. Williams, R. Watts, R. Zeidinger. Daily variation of particulate air pollution and poor cardiac autonomic control in the elderly. Environ. Health Perspect., (1999) 107, pp. 521–525.

S. Lu, R. Duffin, C. Poland, P. Daly, F. Murphy, E. Drost, W. MacNee, V. Stone, K. Donaldson. Efficacy of simple short-term *in vitro* assays for predicting the potential of metal oxide nanoparticles to cause pulmonary inflammation. Environ. Health Perspect., (2009) 117, pp. 241–247.

L. Mikkelsen, M. Sheykhzade, K.A. Jensen, A.T. Saber, N.R. Jacobsen, U. Vogel, H. Wallin, S. Loft, P. Møller. Modest effect on plaque progression and vasodilatory function in atherosclerosis-prone mice exposed to nanosized TiO_2. Part. Fibre Toxicol., (2011) 8, p. 32.

R.C.Murdock, L. Braydich-Stolle, A.M. Schrand, J.J. Schlager, S.M. Hussain. Characterization of nanomaterial dispersion in solusion prior to *in vitro* exposure using dynamic light scattering technique. Toxicol. Sci., (2008) 101, pp. 239–253.

A. Nemmar, P.H. Hoet, B. Vanquickenborne, D. Dinsdale, M. Thomeer, M.F. Hoylaerts, H. Vanbilloen, L. Mortelmans, B. Nemery. Passage of inhaled particles into the blood circulation in humans. Circulation, (2002) 105, pp. 411–414.

A. Pluddemann, C. Neyen, S. Gordon. Macrophage scavenger receptors and host-derived ligands. Methods, (2007) 43, pp. 207–217

D. Porter, K. Sriram, M. Wolfarth, A. Jefferson, D. Schwegler-Berry, M. Andrew, V. Castranova. A biocompatible medium for nanoparticle dispersion. Nanotoxicology, (2008) 2, pp. 144–154.

D.J. Rader, E. Pure. Lipoproteins, macrophage function, and atherosclerosis: beyond the form cell? Cell Metab., (2005) 1, pp. 223–230.

R. Ross. Atherosclerosis: an inflammatory disease. N. Engl. J. Med., (1999) 340, pp. 115–126.

T.M. Sager, D.W. Porter, V.A. Robinson, W.G. Lindsley, D.E. Schwegler-Berry, V. Castranova. Improved method to disperse nanoparticles for in vitro and in vivo investigation of toxicity. Nanotoxicology, (2007) 1, pp. 118–129.

T.M. Sager, V. Castranova. Surface area of particle administered versus mass in determining the pulmonary toxicity of ultrafine and fine carbon black: comparison to ultrafine titanium dioxide. Part. Fibre Toxicol., (2009) 6, p. 15.

A. Seaton, W. MacNee, K. Donaldson, D. Godden. Particles air pollution and acute health effects. Lancet, (1995) 345, pp. 176–178.

V. Sharma, D. Anderson, A. Dhawan. Zinc oxide nanoparticles induce oxidative DNA damage and ROS-triggered mitochondria mediated apoptosis in human liver cells (HepG2). Apoptosis, (2012) 17, pp. 852–870.

A.A. Shvedova, E.R. Kisin, R. Mercer, A.R. Murray, J.V. Johnson, A.I. Potapovich, Y.Y. Tyurina, O. Gorelik, S. Arepalli, O. Schwegler-Berry, A.F. Hubbs, J. Antonini, D.E. Evans, B.K. Ku, D. Ramsey, A. Maynard, V.E. Kagan, V. Castranova, P. Baron. Unusual inflammatory and fibrogenic pulmonary responses to single-walled carbon nanotubes in mice. Am. J. Physiol. Lung. Cell. Mol. Physiol., (2005) 289, pp. 698–708.

W. Song, J. Zhang, J. Guo, J. Zhang, F. Ding, L. Li, Z. Sun. Role of the dissolved zinc ion and reactive oxygen species in cytotoxicity of ZnO nanoparticles. Toxicol. Lett., (2010) 199, pp. 389–397.

J.S. Taurozzi, V.A. Hackley, M.R. Wiesner. Ultrasonic dispersion of nanoparticles for environmental, health and safety assessment—issures and recommendations. Nanotoxicology, (2011) 5, pp. 711–729.

T.C. Tsou, S.C. Yeh, F.Y. Tsai, H.J. Lin, T.J. Cheng, H.R. Chao, L.A. Tai. Zinc oxide particles induce inflammatory responses in vascular endothelial cells via NF-κB signaling. J. Hazard. Mater., (2010) 183, pp. 182–188.

A. Van de Stolpe, P.T. van der Saag. Intercellular adhesion molecule-1. J. Mol. Med., (1996) 74, pp. 13–33.

W. Wu, G. Ichihara, Y. Suzuki, K. Izuoka, S. Oikawa-Tada, J. Chang, K. Sakai, K. Miyazawa, D. Porter, V. Castranova, M. Kawaguchi, S. Ichihara. Dispersion method for safety research on manufactured nanomaterials. Ind. Health, (2013) 52, pp. 54–65.

Y.Y. Xu, J. Yang, T. Shen, F. Zhou, Y. Xia, J.Y. Fu, J. Meng, J. Zhang, Y.F. Zheng, J. Yang, L.H. Xu, X.Q. Zhu. Intravenous administration of multi-walled carbon nanotubes affects the formation of atherosclerosis in Sprague–Dawley rats. J. Occup. Health, (2012) 54, pp. 361–369.

H. Yamawaki, N. Iwai. Mechanisms underlying nano-sized air-pollution-mediated progression of atherosclerosis: carbon black causes cytotoxic injury/ inflammation and inhibits cell growth in vascular endothelial cells. Circ. J., (2006) 70, pp. 129–140.

S.C. Yeh, F.Y. Tsai, H.R. Chao, T.C. Tsou. Zinc ions induce inflammatory responses in vascular endothelial cells. Bull. Environ. Contam. Toxicol., (2011) 87, pp. 113–116.

M.T. Zhu, B. Wang, Y. Wang, L. Yuan, H.J. Wang, M. Wang, H. Ouyang, Z.F. Chai, W.Y. Feng, Y.L. Zhao. Endothelial dysfunction and inflammation induced by iron oxide nanoparticle exposure: Risk factors for early atherosclerosis. Toxicol. Lett., (2011) 203, pp. 162–171.

5. Conclusion

5-1 Cup-type sonicator is suitable to disperse nanomaterials.

Our study described a practical protocol using an indirect cup-type sonicator to prepare nanomaterial suspensions specifically for *in vivo* pulmonary exposure studies. TiO_2 and ZnO nanoparticles, together with MWCNTs were well dispersed in a biocompatible medium and were stable for 7 days after sonication following this protocol. The cup-type sonicator might be recommended as a useful alternative to conventional bath-type sonicator or probe-type sonicator based on its effective energy delivery and assurance of suspension purity.

5-2 ZnO nanoparticles may accelerate atherosclerosis progression *in vitro*.

Exposure to ZnO particles induced cell migration and adhesion of THP-1 cells to HUVECs. The results also demonstrated that exposure to ZnO particles increased macrophage cholesterol uptake due to the upregulation of membrane scavenger receptors of modified LDL. Considered together, the findings suggest that nanosized ZnO particles accelerate foam cell formation, a process crucial in the initiation and progression of atherosclerosis.

5-3 The significance of these studies on the innovation.

These studies contribute to establish the safety index for nanomaterials. The evaluation of safe nanomaterials leads to the progression of nanotechnology. Nanotechnology has the potential to develop new industrial technology and innovation.

6. Acknowledgement

I would like to give heartfelt thanks to Dr. Sahoko Ichihara who provided helpful comments and suggestions. I also thank to Dr. Saeko Tada-Oikawa, Prof. Gaku Ichihara, Dr. Kiyoshi Sakai, Dr. Masako Suzuki, Ms. Kiyora Izuoka, Ms. Kumi Nakao, Ms. Wenting Wu and other coauthors whose opinions and information have helped me very much throughout the production of this study. I would also like to express my gratitude to my family for their moral support and warm encouragements.